Materials Today Sustainability 34 (2026) 101339

Contents lists available at ScienceDirect

Materials Today Sustainability

journal homepage: www.journals.elsevier.com/materials-today-sustainability

Towards sustainable hydrogen infrastructures: Additive manufacturing of metallic materials for enhanced resistance to hydrogen embrittlement

Shengzhao Yang [a], Rongfei Juan [a], Junhe Lian [a,b,*]

[a] Materials to Products, Department of Energy and Mechanical Engineering, Aalto University, Puumiehenkuja 3, Espoo, 02150, Finland
[b] Chair of Forming Technologies, Institute of Metal Forming, RWTH Aachen University, Intzestrasse 10, Aachen, 52072, Germany

ARTICLE INFO

Keywords:
Sustainability
Clean energy
Hydrogen embrittlement
Additive manufacturing
microstructure
Mitigation methods

ABSTRACT

Hydrogen embrittlement (HE) poses a critical challenge to the durability of metallic components in hydrogen infrastructure, threatening the global transition to sustainable and clean energy. Additive manufacturing (AM), with its unique design flexibility, material efficiency, and potential for microstructure control, offers new opportunities to mitigate HE-related degradation. This review focuses exactly on the current state of research at the intersection of AM and HE, highlighting the potential of AM-fabricated metallic materials to enhance performance in hydrogen-rich environments. Applications in aerospace, shipbuilding, and automotive sectors are discussed, emphasizing sustainability gains and production advantages. Uniquely, the review analyzes how key microstructural features of AM materials, such as grain size, dislocation density and dislocation morphology, secondary phases, and molten pool characteristics, influence HE resistance. Furthermore, it evaluates processing strategies, such as multi-material AM and heat treatments, to reduce hydrogen-induced damage. Despite promising advances, knowledge gaps remain in understanding hydrogen diffusion pathways and their interactions with AM-specific microstructures. This article outlines critical future research directions for enabling hydrogen-compatible, AM-based metallic systems, supporting the broader goal of decarbonized energy infrastructures.

1. Introduction

Greenhouse gases (GHGs) generated by fossil fuel combustion and industrial processes threaten global sustainability. This threat has been further exacerbated by the sustained rise in greenhouse gas (GHG) emissions, including N_2O and CO_2, since the mid-19th century (1850) (Fig. 1). Hydrogen, whether gaseous or liquid hydrogen (LH), offers potential to mitigate global warming and pollutant emissions as a clean energy carrier with favorable metrics, particularly its minimal contribution to global warming potential post-energy release. Unlike fossil fuel combustion, which generates global warming gas NO_x and CO_2, hydrogen combustion primarily produces H_2O [3]. Hydrogen energy also possesses various energy-conveying properties, including high energy density [4] and low containment production after energy release [5]. Some research results can demonstrate this conclusion. Corchero et al. [6] found that the fuel consumption of kerosene in aircraft, 31.56 kg/(KN·s), is 2.8 times higher than that of LH. Furthermore, Yusaf et al. [7] pointed out that the utilization of LH rather than fossil fuel can decrease the emission of NO_x gas. Therefore, the advantages offered by LH can potentially drive advancements in the aerospace and automotive industries, potentially serving as a future alternative to fossil fuels in transportation [7]. Recognizing this potential, the European Union has initiated the REPowerEU plan, which aims to invest a substantial sum of 65 billion euros in developing hydrogen infrastructure for the production, importation, and transportation of 20 million tonnes of hydrogen by 2030 [8].

However, it is inevitable for hydrogen embrittlement (HE) phenomena to occur in the storage equipment for hydrogen energy, resulting in premature failure [9]. This premature failure would preferentially happen locally in HE-prone areas (e.g., welding seams, valves, tread lines, end caps), dramatically shortening the life span of storage equipment. The HE also poses a widespread threat to the durability of metallic components [10,11], as shown in Table 1. It leads to premature failure and threatens the sustainability of metallic components serving in other areas, since it could be associated with aqueous environments (such as seawater, rainwater [12], and river water [13], chemistry solutions [14]), or humid air [15]. In 2021, the estimated economic impact of corrosion on equipment and facilities reached up to 6 trillion dollars

* Corresponding author. Materials to Products, Department of Energy and Mechanical Engineering, Aalto University, Puumiehenkuja 3, 02150, Espoo, Finland.
E-mail address: junhe.lian@ibf.rwth-aachen.de (J. Lian).

https://doi.org/10.1016/j.mtsust.2026.101339
Received 2 November 2025; Received in revised form 12 February 2026; Accepted 22 February 2026
Available online 24 February 2026

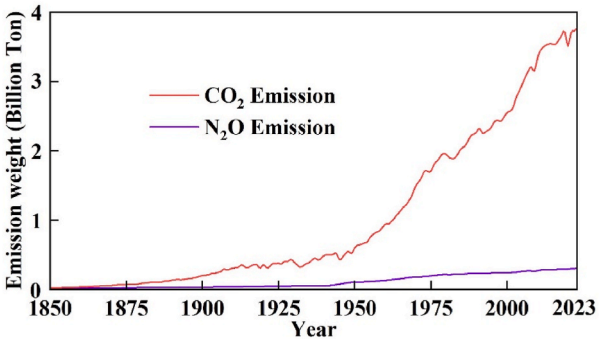

Fig. 1. Annual emission caused by fossil fuel for (a) CO_2, (b) N_2O, (c) global emission for CO_2 and N_2O with year [1,2]. Data and images from the Our World in Data website.

[16], with a considerable share linked to metallic materials and hydrogen embrittlement. The replacement of failed components results in the emission of GHGs (e.g., generating 2.1 t CO_2 for 1 t of new steel [17]). More seriously, HE can result in sudden premature of large-scale buildings, transportation equipment, or facilities without any visible signs [18,19]. Such failures can manifest in vital infrastructure, including bridges, skyscrapers, aircraft, and maritime vessels, resulting in devastating accidents and profound loss of human life. Given the widespread occurrence and huge economic loss of hydrogen embrittlement, researchers have embarked on studying this phenomenon since its early recognition [20]. In 1874, Johnson documented the decrease in the elongation of steel wires caused by HE resulting from exposure to the acidic solution. This early observation of HE highlights its longstanding presence as a challenge in industrial sectors [12]. However, the potential of HE-induced failure in components hindered the application in LH and hydrogen gas.

Luckily, additive manufacturing (AM) has emerged as a novel manufacturing method, offering numerous advantages [21,22]. AM enables the production of components with high structural complexity [23], microstructural flexibility [24], high strength [25,26], and low surface roughness [27]. Moreover, AM allows for the utilization of a wide range of metallic materials and has the potential to significantly reduce waste production and materials consumption [28,29]. In a case study, Top et al. [30] demonstrated that the manufacturing process using a laser-based additive manufacturing system consumed 60.45% less material and resulted in significantly lower CO_2 emissions compared to conventional manufacturing methods. Consequently, AM is poised to replace conventional manufacturing processes (such as casting, forging, and cutting) in response to the call for sustainable development. However, the HE problems have not disappeared in AM-fabricated components [31]. Luckily, the AM provides more opportunities for customers to relieve HE-induced corrosion, as its potentials can be summarized as three points.

(I) High degree of shaping complexity. This merit could enhance the HE resistance of components and assemblies. Compared with the conventional manufacturing process, the design freedom afforded by AM allows for the integration of multiple components into a single structure [32], reducing the number of junctions (such as welding seams [33]) and connectors (such as fasteners and bolts [34]) susceptible to HE. Additionally, the exceptional shaping flexibility of AM provides potential for structural optimization. This optimization could mitigate HE processes accelerated by stress concentrations [35]. It can also eliminate redundant post-processing steps, which may accelerate the hydrogen ingress. For instance, previous studies have demonstrated that post-forging cutting processes can degrade the HE resistance of materials due to the generation of pronounced striations in the cutting-edge area, promoting stress concentration and crack initiation due to the notch effect [36]. Although AM involves thermal cycles similar to welding, the underlying thermal physics

Table 1
Typical examples of metallic materials serving in the hydrogen environment.

Industrial field	Components	Materials	Main fabrication method	Hydrogen sources	Loading Condition
	Combustion Chambers	Cu-Cr-Nb, Inconel 625, and Cu-Cr-Nb/Inconel 625 (Ni-based) bimetallic alloy [45].	Laser powder bed fusion	High-temperature water vapor	950 to 1100 °C, and pressure up to 100 bar [46].
	Hydrogen storage cryogenic vessels	2219 Al alloys, 2A14 Al alloy, and 2219 Al-Cu alloy, CoCrFeMnNi high-entropy alloy [47].	Rolling, welding	Liquid hydrogen	20.35 K at 1 bar [48].
	Fuselage for commercial flight	Al7075 alloy [49].	Stamping	Rainwater, humid air	When cruising at around 12000 m, the sujectsed stress is about 25 to 45 MPa [50].
	Propeller shaft	17-4 PH martensitic stainless steel [51].	Cutting, molding	Seawater	Bearing the torsional load, axial thrust, and bending load [52].
	Ship hull	Carbon steel St41, steel 15G2ANb (AH36), and steel 17HNMBVA (E690) [53].	Rolling, welding	Seawater, humid air	Bearing the hull deflections, vertical bending moment, and wave-induced load [54].
	Ship deck	EH36 low-carbon and low-alloy steel [55].	Rolling, welding	Seawater, humid air	Bearing cargo loads and wave-induced loads [56].
	Car body	MS-AHSS steel [53].	Stamping	Rainwater, humid air, pickling acid liquid	Bearing the static stiffness loads and cyclic loads [57].
	Fasteners	316L stainless steel, 60Si2Mn spring steel [34].	Forging, cutting, drilling	Rainwater, humid air	Bearing the pre-load and cyclic load [58].
	Hub bolt	Zinc-coated SCM435 steel, USIBOR 1500® steel, and USIBOR 2000® steel [38].	Forging, cutting	Rainwater, humid air	Bearing the pre-load and cyclic load [58].
	Hydrogen-storing fuel cell	silica-sphere-coated aluminum alloy 7075 [59].	Casting	Gas hydrogen	700 bar at ambient temperature [60].

differs significantly. AM processes, particularly laser powder bed fusion, exhibit cooling rates orders of magnitude higher (10^5 to 10^6 K/s) compared to conventional welding. This rapid solidification suppresses the formation of coarse, segregated microstructures often found in the heat affected zones (HAZ) of traditional welds, which are typical initiation sites for hydrogen cracking. Furthermore, the process is free from constraints imposed by joining semi-finished components [37]. This freedom enables AM-fabricated samples to replace macroscopic heterogeneous weld joints with microscopic, homogeneously distributed melt pools, thereby achieving optimized microstructures and reduced residual stress concentrations that decrease the overall sensitivity to HE.

(II) The excellent fabrication flexibility. The strength of AM helps impede the diffusion of hydrogen atoms into the substrate. In the past, ceramic coatings (e.g., Zinc [38] and silica-sphere [39]) have been applied to protect metallic substrates from HE corrosion, but the coating process will also introduce hydrogen atoms into the metallic matrix. For example, Xu et al. [38] observed HE-induced cracks in the fracture surface of zinc-coated SCM435 steel, attributing it to the Zinc electroplating process, which introduces hydrogen atoms into the iron-based alloy matrix. Furthermore, traditional coating processes are challenging to implement on components with intricate geometries [40]. Fortunately, the advent of multi-material additive manufacturing (MMAM) enables the fabrication of ceramic-metal composite components without the need for post-treatment processes [41], or it can modify the microstructure of susceptible areas [42] to alleviate HE corrosion. Nevertheless, the application of MMAM in preventing HE corrosion remains an underexplored research area.

(III) Possibility in microstructure optimization. The AM process produces components with distinct microstructures compared to those fabricated via conventional manufacturing methods, which can lead to improved resistance to HE. For example, Baek et al. [43] observed that the AM process significantly improved the HE resistance of 304L austenitic stainless steel compared to rolled 304L. While decreases in HE resistance have been observed in other materials [44]. This finding offers a new avenue for mitigating HE-related challenges, which will be further discussed in detail in the subsequent sections.

In this article, the authors will first summarize the AM methods and application scenarios, as well as the investigation methods of components serving in hydrogen environments. These aspects are helpful for readers to gain a clear understanding of the service conditions of materials exposed to HE and to establish suitable research targets for subsequent AM-related studies. Then, the research progress on the microstructure of AM-fabricated materials serving in hydrogen environments will be introduced. Finally, this review will prospect future development and highlight the deficiencies in current research.

2. AM methods for metal shape-formation

Fig. 2 shows the classifications of AM methods for metal forming. Within the scope of the current review, the investigation of metallic components for HE primarily focuses on those manufactured using powder bed fusion (PBF) and direct energy deposition (DED) methods. Consequently, this chapter will place greater emphasis on PBF and DED, while acknowledging the vast research potential of other AM techniques.

2.1. Powder bed fusion

On the bias of beam type, PBF can be further subdivided into two categories: (1) laser powder bed fusion (LPBF), and it is also known as selective laser melting (SLM) or selective laser sintering. (2) Electron-beam powder bed fusion (EPBF). In the PBF process, the powder is transferred from the powder chamber to the building chamber via a scrapper. Subsequently, a laser or electron beam is employed to fuse the powder particles, resulting in the formation of components. The powder plates and building chamber move in synchronized motion, with the powder feeding rate and layer thickness determining their respective vertical movements. This powder-feeding model utilized in PBF enables the conveyance of fine powder particles with a small average diameter (typically below 20 μm [45,46]) into the building chamber (Fig. 3a), which contributes to shaping workpieces with high precision. A detailed explanation and comparison with DED for this characterization will be elaborated in Section 2.2. Additionally, unlike conventional casting or forging processes, the PBF method enables in-situ monitoring to detect defects and analyze the microstructure during the formation process, providing valuable data for parameter optimization [47]. However, it is important to note that the size of the PBF machine significantly limits the volume of the components that can be produced [48].

2.2. Direct energy deposition

Lots of processes can be categorized in DED methods, including laser metal deposition (LMD), laser cladding (LC), and wire arc additive manufacturing (WAAM). Similar to PBF, DED can be easily integrated with in-situ monitoring systems. The fabrication process of DED, as illustrated in Fig. 3b and c, can be summarized as follows [47]: (1)The first step involves melting wire or powder using focused thermal energy, which can be provided by wire arc, laser, or electron beam. (2)The melted material is deposited as heat droplets onto the surface of the substrate or printed components. (3)The droplets undergo solidification to form the final structure.

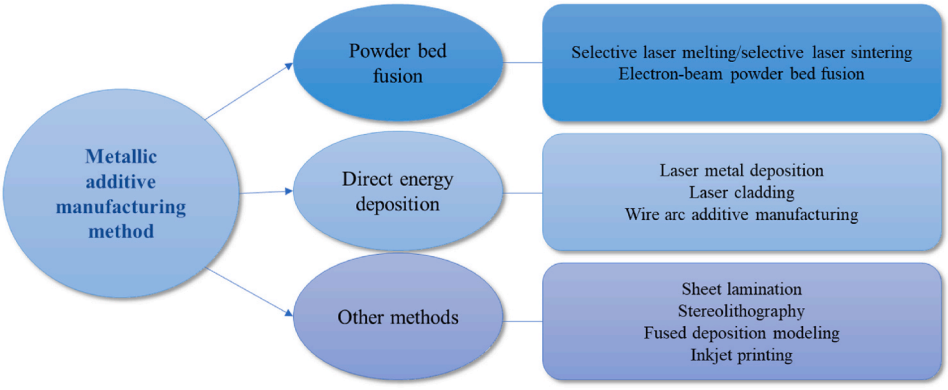

Fig. 2. Classifications of AM methods for metal forming.

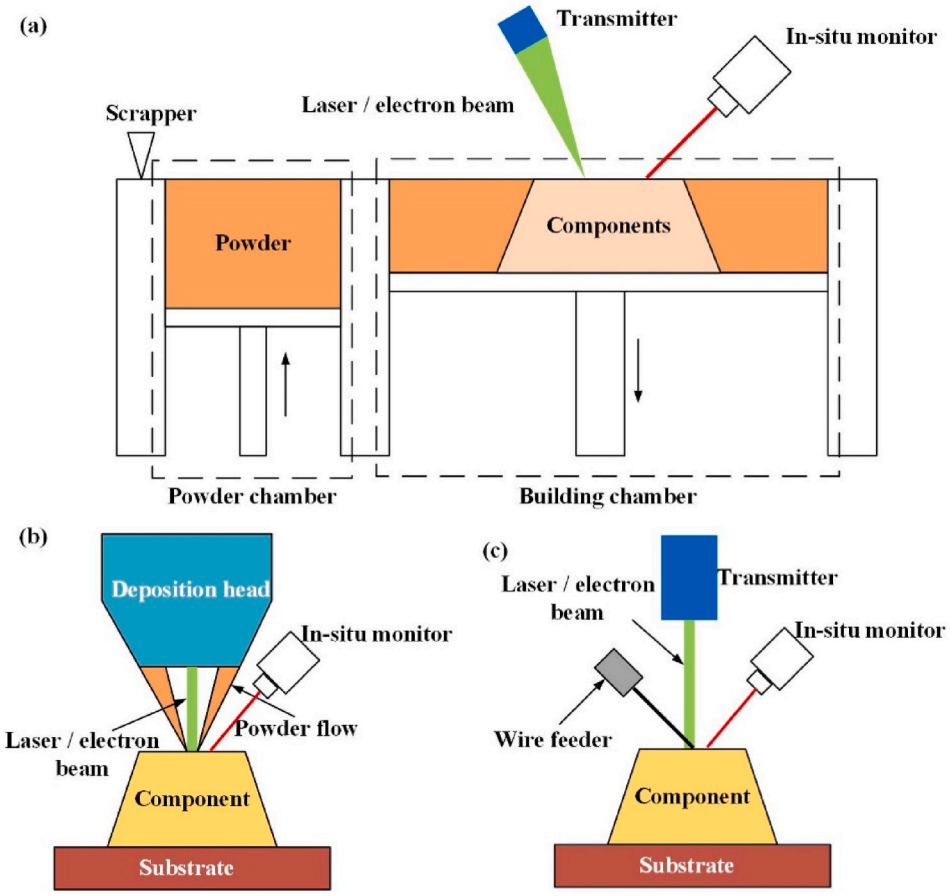

Fig. 3. Schematic drawings of different AM methods. (a) PBF, (b) DED with powder feeding system, (c) DED with wire feeding system.

2.3. Other methods

1. Sheet lamination (SL)

SL uses a roller to compress metallic sheets and bind them into one integrity sheet by sheet [49]. As it is a relatively new method for printing metallic components, there has been limited research conducted on this technique.

2. Stereolithography (SLA)

Before the SLA process, the metallic powder was mixed with photo-polymerizing resin to create a printable suspension [50]. During printing, the suspension is exposed to ultraviolet light emitted by a transmitter, causing it to solidify layer by layer. After the SLA process, components are removed and heated in a furnace to eliminate residual resin. However, SLA-fabricated components often exhibit high porosity rates [51], resulting in poor HE resistance and mechanical properties. Further improvements are necessary to enhance their performance.

3. Fused deposition modeling (FDM)

FDM involves the deposition of polymer/metal filaments onto a substrate to fabricate components [52]. Subsequently, the components are sintered in a furnace to remove the polymer. Similar to SLA, FDM is susceptible to producing porous samples.

4 Inkjet printing

In the inkjet printing process, a liquid (such as polymer/metallic suspension or metallic salt) is expelled from a nozzle onto a building plate [53]. The printed samples are then solidified either through heat curing or by projecting ultraviolet light to achieve compact components. However, the high porosity rates observed in inkjet printing-fabricated components hinder their application in hydrogen environments [54].

3. Application scenarios

Among many industrial sectors, the aerospace, shipbuilding, and automotive industries are representative and popular application scenarios for AM materials with the HE concerns, as demonstrated in Table 1, and additionally show current and potential applications of AM technologies and components. Specifically, the aerospace industry represents a critical sector where AM has achieved substantial adoption due to high-performance demands, the necessity for lightweight structures, and complex geometries that traditional manufacturing methods struggle to achieve efficiently. Shipbuilding, with its nature aggressive, hydrogen-rich marine environments, has also shown a rapidly increasing interest and adoption potential of AM, especially for large-scale components. Finally, the automotive industry, while currently exhibiting a lower adoption rate of AM technologies, also shows substantial potential for growth in AM adoption, especially in applications targeting weight reduction and enhanced manufacturing flexibility. Following the progressive trend across these industries, they will be individually addressed in the following.

3.1. Components of the aerospace industry

In the aerospace industry, the demanding service requirements and complex component topologies in hydrogen environments create

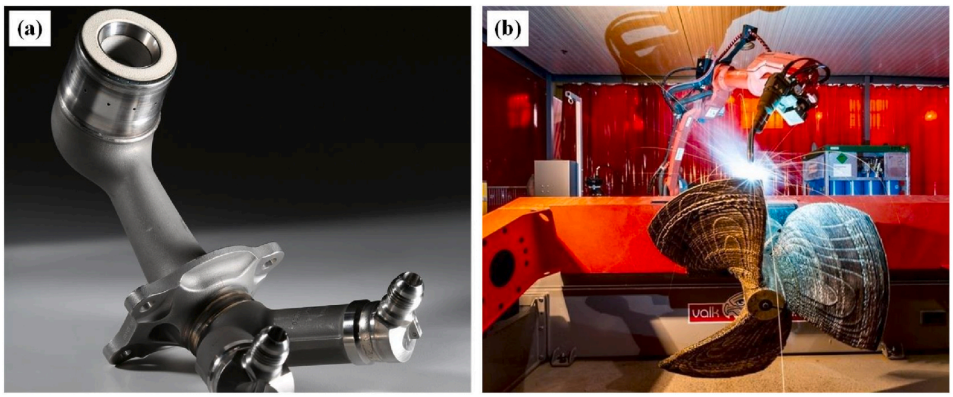

Fig. 4. (a) Fuel nozzles produced by General Electric, reproduced with permission from Colibrium Additive. (b) propeller fabricated by RAMLAB company via WAAM, reproduced with permission from RAMLAB and Damen Shipyards.

difficulties for traditional processing methods but offer ample opportunities for AM. Notably, AM has already been adopted for the large-scale production of aerospace parts. General Electric (GE) company, for instance, utilized AM to produce over 30,000 fuel nozzles for aerospace companies in 2018, as shown in Fig. 4a [55]. Nevertheless, it is important to acknowledge that the HE problem persists even with the utilization of AM for component fabrication. Balancing HE resistance and other essential service properties often involves trade-offs. For instance, the addition of excessive chromium elements to GRCop-42 Cu-based alloy, fabricated via AM, may enhance HE corrosion resistance but diminish its thermal diffusion rate [56].

Despite this, the aerospace industry holds considerable potential for the application of AM technology. The increasing utilization of LH as a propellant in aerospace systems has amplified the demand for LH flaring and storage systems, which necessitate materials with enhanced properties but often come at higher costs [57]. In this situation, AM presents a promising solution by reducing material consumption and overall costs. Unlike fossil fuels, LH must be stored at cryogenic temperatures (approximately 20.46 K) to maintain its liquid state and minimize vessel storage volume. Additionally, high-pressure vapor water at elevated operating temperatures can lead to HE. For example, combustion chambers experience service temperatures of up to 3041.85 K and are subjected to HE from high-pressure water vapor during ignition [57]. Expensive Al-based alloys (e.g., 2219 Al alloys, and 2219 Al-Cu alloys [58]) for the cryogenic environment, Nickel-based (e.g., Inconel 625 [59], Hastelloy X [60]), and steel-based superalloys (e.g., A-286, JBK-75 [61]) for the high-temperature environment must be applied, but significantly increase the production cost. Furthermore, the integration of Cu-based alloys with Ni-based or iron-based alloys has been proposed to facilitate heat diffusion and protect combustion chambers, a task that proves challenging with traditional manufacturing methods [56]. Thus, the complex structures and stringent material requirements of LH storage and igniting components have garnered significant attention from engineers and researchers in the field, who recognize the potential of AM to address these challenges. NASA, a pioneering institution in the aerospace industry, has already embraced AM methods for fabricating spaceflight components intended for LH environments. These components include combustion chambers, pump volutes, and liquid fuel pumps [62]. Notably, certain AM-fabricated components have been incorporated into the RS-25 rocket, which features an LH engine. In summary, the trend of utilizing AM for fabricating components in LH-fueled propulsion systems is gaining momentum within the aerospace industry, driven by the need to overcome HE corrosion challenges and meet the stringent material requirements of LH storage and igniting components.

3.2. Components of the shipbuilding industry

The shipbuilding industry faces unique challenges compared to the automotive and aerospace industries. One significant difference is the longer lifespan and extended exposure to moisture for ships. While household vehicles typically have an average lifetime of around 12 years, ships can last for 30 to 50 years, with the majority of their service time spent on water [63]. The prolonged exposure to water or moisture in the marine environment makes ship components more susceptible to HE corrosion. In contrast, although commercial airplanes have a lifespan of up to 40 years, their actual service time is shorter and determined by flight hours [64]. In addition, production costs rather than service properties are more important than those in the aerospace industry, since less demanding service environment.

Despite this, AM technology holds the potential to meet the demands of shipbuilding industries operating in hydrogen environments. The inherent customization capabilities of AM align well with the high-cost and low-quantity nature of components required for large ocean freighters, such as scupper plugs, which are susceptible to hydrogen ingress from seawater [65]. In 2022, Berge Mafadi utilized AM-fabricated scupper plugs for its cargo. Traditional manufacturing methods for scupper plugs are expensive, given the need for engineer-designed, non-generic shapes to prevent contaminant or water leakage [66]. Thus, the high forming flexibility of AM is suitable for producing scupper plugs rather than casting or forging. Moreover, AM exhibits remarkable capabilities in fabricating ship components with intricate structures but limited dimensions, such as engines and propellers [67]. Unlike aerospace components, shipbuilding industry requirements do not heavily prioritize forming precision and surface roughness. Consequently, WAAM is commonly employed in shipbuilding, since it excels in producing large-scale parts at lower production costs compared to PBF or DED methods. RAMLAB company successfully manufactured propeller shafts with a diameter of 1.35 m via WAAM (Fig. 4b), which were installed in the Stan Tug 160 ships [68], highlighting WAAM's ability in commercial shipbuilding applications. In another case, DNV produced 2-m diameter ship propellers and Panama chocks using WAAM, demonstrating twice the yield strength of their cast counterparts [69]. Considering the undersea service environment of propellers, the HE resistance must be considered for those WAAM-fabricated propellers. Regrettably, due to commercial confidentiality, the specific HE resistance capabilities of the aforementioned AM-fabricated components in their intended application scenarios remain undisclosed.

The advantages of AM extend to its potential for producing spare parts during voyages. Recognizing that maritime ships may require extended periods of navigation without external supply for replacement accessories, the US military initiated a project exploring the fabrication of spare parts at sea using wire-feed AM [70]. While the entry of

hydrogen from seawater and humid air may potentially impact the service properties of AM-fabricated spare parts, it is not clear what the result of this project will be [70]. In conclusion, AM holds significant application prospects in the shipbuilding industry. However, researchers and producers need to address HE-related challenges stemming from water and humid air to ensure the optimal performance of AM-fabricated components in maritime environments.

3.3. Components of the automotive industry

HE has been a persistent challenge in the automotive industry due to the frequent exposure of vehicle components to HE-inducing environments, such as rainwater, humid air, and detergents [71]. Hydrogen atoms can also permeate into inner components through openings, permeable materials, or moist air [71]. As a result, automotive companies often resort to using low-strength steels in fasteners and other components, leading to a significant increase in vehicle weight [26], as steels with an ultimate tensile strength exceeding 1000 MPa are susceptible to HE corrosion [47]. HE-induced degradation can occur not only during the service life of the vehicle but also during post-treatment processes. Surface treatments like acid cleaning and electroplating, commonly applied to vehicle components, can introduce hydrogen atoms into the metallic matrix, potentially compromising the fatigue resistance of components [34]. Therefore, HE is a critical challenge hindering the development of the automotive industry. However, given that the majority of automotive consumers are individual citizens, companies and their research teams must strike a balance between HE resistance and material cost [72]. Consequently, many vehicle components are made of cost-effective stainless steel with a level of HE resistance that meets the requirements. In addition, traditional processing methods continue to maintain their dominant position in the automotive industry, since the low fabrication efficiency of AM currently hinders its widespread adoption in the automotive industry for mass production [73]. Nevertheless, some efforts have already been initiated. BMW has begun small-series production of the iX5 Hydrogen model, powered by hydrogen energy, and has reported that some components are manufactured using AM [74]. Despite this, restricted by the limited application and investigation of AM in the automotive industry, there is a lack of comprehensive investigation into the service properties (e.g., lifespan and operational efficiency) of AM-fabricated components in hydrogen environments. This presents an emerging area of interest for engineering research.

3.4. Other application scenarios

The high production costs, lengthy production times, and limited production volumes hinder the widespread adoption of AM. In addition, the unique characteristics of different industries further impede the application of AM. For example, the project-based nature of civil engineering operations makes it less suitable for the rapid implementation of AM technology [75]. Nevertheless, this does not undermine the significance of future research on AM in other industrial sectors.

One area where the potential of AM is evident is in the repair of large-scale facilities or equipment operating in hydrogen environments. AM has already been successfully employed in repairing components with HE-induced damage across various industries, including aircraft landing gear [76], ship propellers [67], aircraft fuselage [76], car bodies [76], nuclear reactors [77], and so on. However, in some cases, the repair process itself may occur in a hydrogen environment, such as underwater facilities. Previous studies [78] have highlighted that underwater repair processes introduce hydrogen into the materials, resulting in the formation of large cracks, high surface roughness, and other issues. Researchers have made attempts to address this challenge by implementing strategies to block the entry of hydrogen. Some attempts to block the entry of hydrogen have been conducted by researchers. Wang et al. [79] developed an innovative underwater direct energy deposition (UDED) setup to repair pre-existing cracks immersed in water, as exhibited in Fig. 5; they designed a gas curtain nozzle to create a dry air cavity during the UDED process, effectively preventing hydrogen diffusion. The maximum hydrogen content observed in all samples was 0.618 ml/100g at a water depth of 150 mm, significantly below the welding standard of 5 ml/100g. Guo et al. [80] increased the protection gas area by modifying the flux-core wire component (replacing 60% of Ca2F powder with rutile powder) in the WAAM

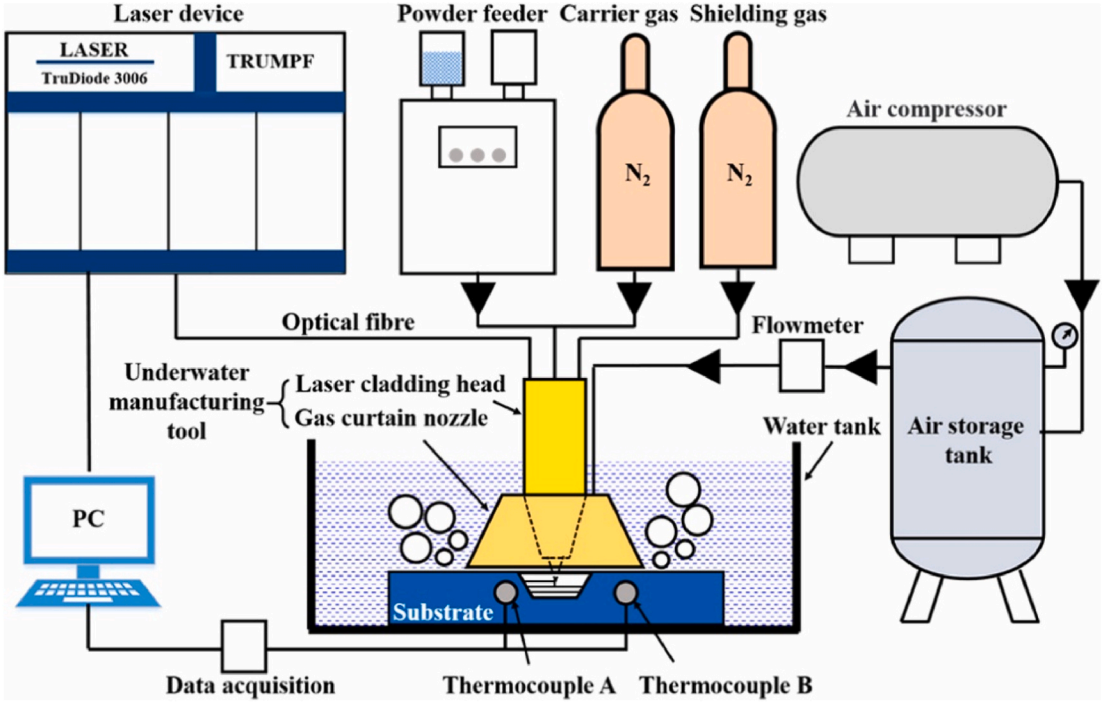

Fig. 5. Schematic diagram of the UDED repairing system [79].

process. This improvement resulted in a 65% reduction in the remaining hydrogen content in the printed 304 stainless steel samples. Unfortunately, AM methods for repairing components in hydrogen environments have not yet gained widespread use in engineering and should be the focus of future research endeavors.

4. Mechanisms and investigation methods of hydrogen embrittlement

4.1. Mechanisms

The main fundamental mechanisms underlying HE in AM-fabricated materials are similar to those observed in traditional processing methods, and the main HE mechanisms are summarized shortly as follows. It is important to note that these mechanisms may not individually impact the mechanical properties but can collectively contribute to the overall service performance [81].

1 Hydrogen-enhanced localized plasticity (HELP)

This theory suggests hydrogen atoms would enhance dislocation mobility, thus softening materials and accelerating the failure process, as hydrogen reduces the energy barrier for dislocation gliding by being inserted into the matrix. This phenomenon was demonstrated through atomic simulations by Huang et al. [82], and their in-situ transmission electron microscopy (TEM) for α-Fe. In addition, hydrogen accumulates in regions with high tensile hydrostatic stress and increases the dislocation mobility in this area, such as crack tips [83]. The promoted dislocation movement softens the matrix in crack tips, accelerates crack propagation, and leads to the premature failure of the material. Conversely, Xie et al. [84], using in-situ TEM, observed that dislocation motion in pure Al was dragged and impeded during cyclic compression after hydrogen charging. Song and Curtin [85] reported this drag effect in α-Fe through atomic simulations. Huang et al. explained this apparent contradiction by attributing it to the significantly lower hydrogen concentration in their experiment compared to earlier studies [82]. Therefore, the applicability of the HELP mechanism is limited and can only explain HE in specific cases.

2 Hydrogen-enhanced decohesion (HEDE)

The HEDE mechanism was first proposed by Pfeil et al., in 1926 [86,87], and it has been the most accepted theory in HE study. This mechanism suggests that hydrogen diffuses into the matrix and accumulates to high concentrations during the hydrogen charging process, significantly weakening atomic bonding strength and reducing the material's overall strength [88,89]. The atomic-scale mechanism was further elucidated through simulations conducted by Hu et al. [90], which demonstrated that hydrogen increases the electron density at interstitial sites, thereby enhancing Pauli repulsion. This effect leads to lattice expansion and the weakening of atomic bonds. Localized degradation is further exacerbated by hydrogen accumulation in specific regions, such as grain or phase boundaries, vacancies, twins, sites of maximum hydrostatic stress, crack tips, and dislocations [86]. This localized weakening can be quantitatively described by the following equation [86,91]:

$$\sigma_H = \sigma_0 - aC \tag{1}$$

where σ_H is the local critical cohesive stress decreased by HEDE; σ_0 is the critical cohesive stress in a hydrogen-free environment; C is the hydrogen concentration, and a is a parameter related to the loss of cohesive stress due to the HEDE process. According to this model, premature failure occurs when the local stress exceeds σ_H as a result of hydrogen accumulation.

3 Adsorption-induced dislocation emission (AIDE)

Proposed by Lynch in 1976 [92], the AIDE theory is the combination of HEDE and HELP [81]. During service, hydrogen accumulates in the crack tip region due to stress concentration. According to the HEDE mechanism, this accumulation reduces atomic cohesive strength, weakening the material. Simultaneously, the HELP mechanism suggests that hydrogen lowers the energy barrier for dislocation glide, promoting dislocation emission under the influence of hydrogen. This emission facilitates localized strain near the crack tip, leading to the formation of microvoids. The interplay between these two degradation processes ultimately accelerates crack propagation and results in premature failure.

4 Hydrogen-enhanced strain-induced vacancies (HESIV)

In 2004, Nagumo [93] first introduced the HESIV mechanism. This theory proposes that hydrogen reduces the formation energy of atomic-scale vacancies during the straining process, thereby accelerating strain-induced vacancy generation and promoting the formation of vacancy clusters [94]. Stabilized by hydrogen, these clusters subsequently merge into microvoids, facilitating their growth and ultimately leading to premature failure of the material.

5 Metallic hydride formations

When hydrogen is charged, the matrix or precipitation phases can absorb hydrogen atoms and form new phases when the hydrogen content exceeds the solubility [83]. This results in the transformation into more brittle phases. For example, the NiTi intermetallic compound can absorb hydrogen from HE-induced liquid, transforming into a brittle NiTiH phase [95]. Those brittle phases can accelerate crack propagation or become the initiation points for cracking due to stress concentration.

6. Hydrogen molecule recombination

This theory suggests that hydrogen atoms can be absorbed onto the surface of samples from the hydrogen environment. These surface-absorbed hydrogen atoms then migrate into the matrix, where they recombine to form H_2 within pores and cracks [96]. This process increases the gaseous pressure in these areas, initiating crack initiation or propagation. Consequently, the recombination of hydrogen atoms severely degrades the mechanical properties of materials.

4.2. Mechanical testing methods

Comparative mechanical testing of hydrogen-charged and hydrogen-free samples is an effective approach to quantify hydrogen-induced degradation and mitigate the risk of catastrophic failure before materials are deployed in service. However, the method of hydrogen charging remains a challenging question for researchers. Currently, hydrogen charging techniques can be broadly classified into three categories: electrochemical hydrogen charging, gaseous hydrogen charging, and tubular hydrogen charging, as illustrated in Fig. 6. Among these, electrochemical hydrogen charging is the most widely adopted method due to its straightforward and accessible process. Gaseous hydrogen charging is typically used to investigate the hydrogen behavior of samples in high-pressure hydrogen gas environments. However, the complexity and expense of high-pressure autoclaves required for gaseous charging limit their application to a relatively small number of research groups [97]. Tubular hydrogen charging, on the other hand, is versatile as it enables charging with either high-pressure hydrogen gas or liquid hydrogen under cryogenic conditions. Compared to gaseous hydrogen charging, this method consumes a smaller volume of hydrogen gas. Nevertheless, the application of tubular charging is constrained by the hollow structure of test samples, which restricts the miniaturization and flexibility of testing AM-fabricated samples with high production costs.

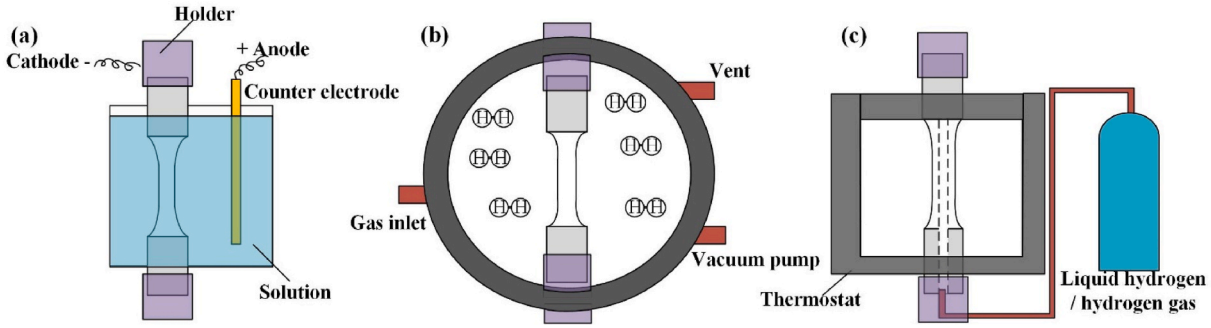

Fig. 6. (a) Electrochemical hydrogen charging, (b) gaseous hydrogen charging, (c) tubular hydrogen charging.

Despite the limitations of these charging methods, they can be effectively coupled with various mechanical testing techniques for both in-situ and ex-situ evaluations. These mainstream testing methods can be categorized as follows.

1 Tensile tests

To quantify the loss of tensile properties caused by HE, slow strain rate testing (SSRT) and linearly increasing stress testing (LIST) are now widely adopted by researchers [81]. As for SSRT, specimens will be stretched with a constant increasing elongation, while specimens will be stretched with a slow-increasing load in LIST tests [81]. In both tests, specimens are elongated until a fracture occurs in different hydrogen environments. As for the hydrogen environment, the electrochemical hydrogen charging solutions typically consist of H_2O as the solvent and various solutes, such as $NaAgO_2$ [98], H_2SO_4 [99], and $NaAsO_2$ [99]; for the gaseous charging, the hydrogen gas is generally made of pure water vapor or H_2 with high pressure. However, in some research, impurities (such as O_2 and H_2S) are added to hydrogen gas for further investigation. As experimental results, the elongation, yield strength, ultimate tensile strength (UTS), and reduction of fracture area (RA) after tensile tests in the hydrogen-free environment (h_1), and hydrogen charging (h_2) will be used to get h_{Loss}, which can be used to quantitatively determine the HE resistance of materials and calculated by the formula [100,101]:

$$h_{Loss} = \frac{h_1 - h_2}{h_1} \times 100\% \quad (2)$$

2 Electrochemical nano-indentation tests (ENIT)

To investigate the influence of hydrogen diffusion on the shear properties of materials, researchers have developed an ENIT technique. In the testing process, the test sample is first immersed in a solution that induces HE, and then hydrogen is introduced into the sample under a cathodic potential. To assess the degradation caused by hydrogen diffusion, the test samples are also subjected to anodic potential charging to facilitate the desorption of hydrogen from within the material. This serves as a counterpart experiment to evaluate the effects of hydrogen on the material. After the charging process, nanoindentation testing is performed to obtain load-displacement curves, from which various parameters can be extracted. These parameters include the maximum shear stress [102] and pop-in load [103], which helps determine the impact of hydrogen diffusion.

3 Fatigue tests

In fatigue testing, hydrogen significantly accelerates crack growth rates, leading to premature failure [104]. Hydrogen-induced degradation can be evaluated by comparing the crack growth rate in air and hydrogen environments. To quantify the fatigue resistance of metallic materials, pre-cracks are typically introduced into the test samples before testing [104]. Then, the crack growth rate per cycle ($\frac{da}{dN}$) is then calculated based on variations in voltage across the cracks. To illustrate the fatigue crack growth process, plots of ($\frac{da}{dN}$) versus the number of cycles (N_f) or stress intensity factor (Δ K) are commonly used. Compared to hydrogen-free samples, hydrogen-charged samples generally exhibit lower maximum N_f and Δ K, but higher maximum ($\frac{da}{dN}$). These differences highlight the detrimental impact of hydrogen on the fatigue behavior of metals.

4 Charpy impact tests

Charpy impact testing is a simple yet cost-effective method for determining the impact toughness properties of metallic materials, which is crucial for assessing the reliability of hydrogen storage materials, particularly those exposed to liquid hydrogen environments [105]. Test specimens are typically prepared as long strips with a V-shaped notch. Within the scope of the authors' review, Charpy impact testing is predominantly conducted under ex-situ hydrogen charging conditions, as the testing process would otherwise damage the charging equipment. In this method, hydrogen-charged samples are removed from the charging cell and subjected to impact by a pendulum released from a known height. The stiffness of the sample can be quantitatively evaluated by calculating the energy absorbed during the impact. The degree of hydrogen-induced degradation (E_{loss}) can be expressed as:

$$E_{loss} = \frac{E_h - E_0}{E_0} \times 100\% \quad (3)$$

where E_h represents the energy absorbed by the hydrogen-charged sample, and E_0 denotes the energy absorbed by the hydrogen-free sample.

4.3. Measurement methods for hydrogen diffusion, concentration, and distribution

1 Thermal desorption spectroscopy (TDS)

Fig. 7a illustrates the mechanism of TDS. When heating specimens in the air-lock vacuum chamber (AVC), hydrogen will desorb from different trap sites at the corresponding temperature, be pumped into the ultra-high vacuum chamber (UVC), and finally be detected by spectroscopy. This process helps clarify the type and hydrogen capture extent of each hydrogen trap site in materials. The heating rate (φ) of the TDS experiment can affect the corresponding temperature and the trap activation energy (E_a) of the trap site. Therefore, to calculate the activation energy, multiple heating rates are needed [109]:

$$\frac{d\left(\ln\left(\varphi/T_p^{\,2}\right)\right)}{d\left(T_p^{\,-1}\right)} = -\frac{E_a}{R} \quad (4)$$

where T_p is the temperature of the hydrogen desorption peak and R is

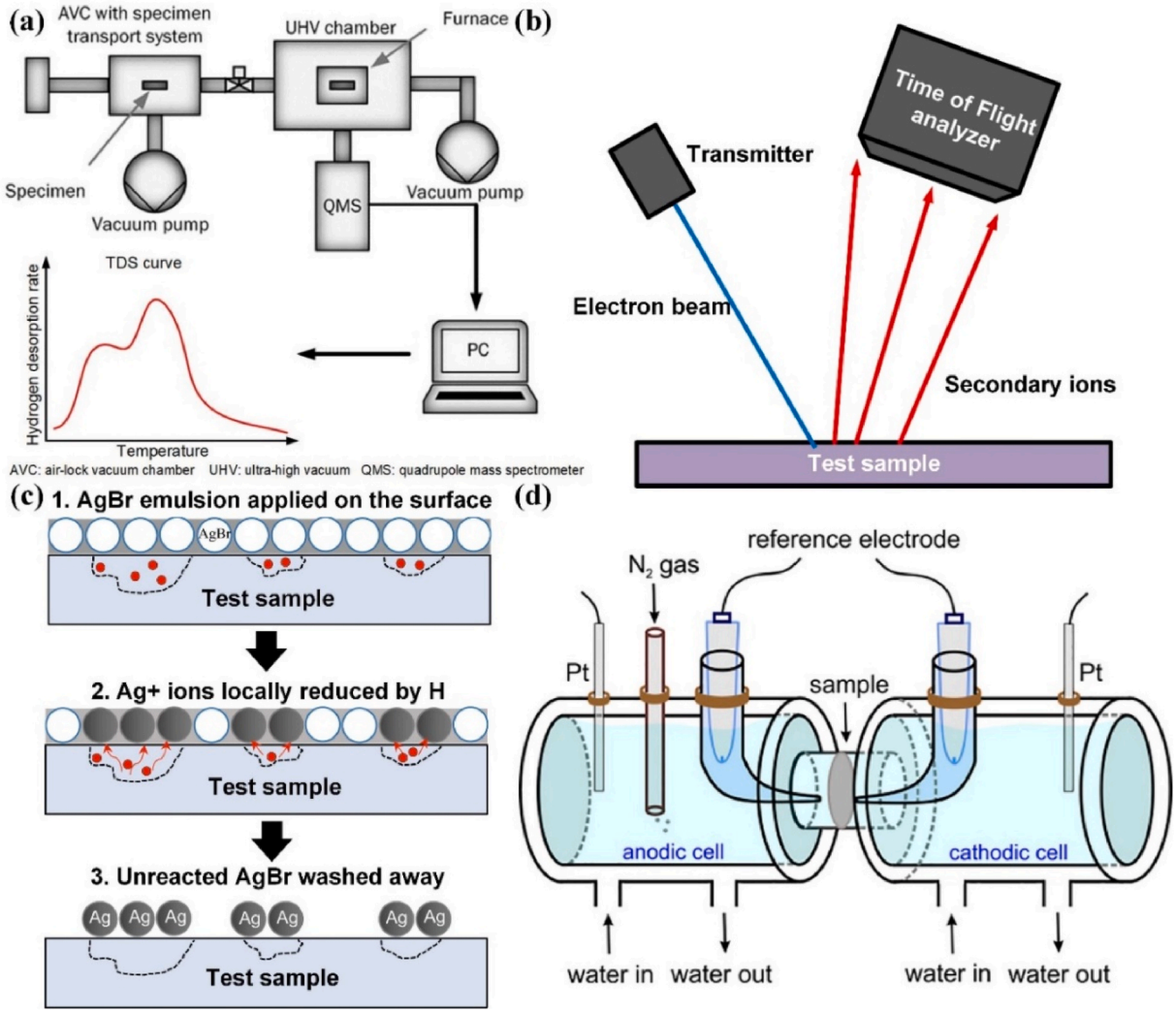

Fig. 7. Schematic diagram of different hydrogen distribution detection methods. (a) TDS [106], (b) ToF-SIMS, (c) HMT [107], (d) HPT [108].

the universal gas constant. Usually, at least three TDS tests with different φ are conducted to draw the ln (φ/T_p^2) versus T_p^{-1}, then get the slope of the plot ($k = -\frac{E_a}{R}$) via the least square method, and finally get the value of E_a.

2. Time-of-flight secondary ion mass spectrometry (ToF-SIMS)

With the help of ToF-SIMS, the distribution of hydrogen and its corresponding hydrogen content can be detected precisely, as depicted in Fig. 7b. In the ToF-SIMS test, the ion beam is emitted to bombard the surface of the test sample, getting the secondary ion, and finally determining the distribution and content of the element by analyzing the flight velocity of the secondary ion [110]. The presence of ToF-SIMS can remedy the shortcoming of energy-dispersive X-ray spectroscopy (EDS), which is commonly used for detecting elemental distribution but hard to detect elements with low atomic numbers (<11) precisely [111].

3. Hydrogen microprinting technique (HMT)

Compared with TDS, the HMT can reveal the hydrogen distribution more deeply and precisely, and the mechanism is shown in Fig. 7c. During the HMT process, the test specimens will be immersed in the AgBr emulsion [112]. Then, the escaped hydrogen will react with AgBr; the Ag + ions will be transformed into Ag and left in the position where they react with hydrogen. After HMT treatment, the hydrogen diffusion paths can be determined by tracking the distribution of Ag atoms via scanning electron microscopy (SEM) and transmission electron microscopy (TEM).

4 Hydrogen permeation test (HPT)

The HPT is a straightforward method used to compare the hydrogen diffusion resistance of different materials [81]. The experimental setup for HPT is depicted in Fig. 7d. Under the influence of electrochemical forces, hydrogen diffuses from the hydrogen input side, through the tested metal sheet, and eventually enters the hydrogen output side. By measuring the hydrogen charging current density, the rate of hydrogen absorption by the test samples can be calculated, yielding results that are consistent with those obtained from TDS tests [113]. The calculating formula will be changed with the variation of test solutions. For specimens exposed to a high-pressure air environment in the HPT, the hydrogen input side is filled with hydrogen gas rather than a hydrogen solution. Nevertheless, the underlying mechanism is similar to that of the hydrogen solution HPT.

5. Microstructures affecting the HE resistance properties of AM-fabricated materials

The unique microstructure of AM materials has attracted considerable attention from researchers, as it plays a critical role in determining

the service life of components exposed to hydrogen environments. The rapid solidification rates inherent to AM, up to 10^6 K/s [114], generate a hierarchical microstructure that fundamentally distinguishes AM alloys from their conventionally manufactured counterparts. While AM materials share common metallurgical features such as grain size and dislocation density, these conventional factors are often superimposed with unique AM-specific characteristics that alter the physical mechanisms of HE. Specifically, the repeated melting and solidification cycles introduce mesoscopic melt pool boundaries (MPBs) and cellular segregation networks that act as distinct hydrogen traps or diffusion highways, differing significantly from the random dislocation tangles or equilibrium grain boundaries found in casting or forging. Furthermore, the strong thermal gradients induce preferential crystallographic textures and spatial orientations of grains that allow for the engineering of hydrogen diffusion paths, creating a complex interplay where HE resistance is determined by the competition between conventional trapping mechanisms (e.g., grain refinement) and unique solidification artifacts (e.g., MPB segregation). Consequently, understanding the influence of microstructural characteristics on HE is essential for developing effective strategies to enhance the durability and sustainability of such components.

5.1. Grain size

The grain size is a crucial factor influencing the HE resistance of materials, as it affects the gross length of grain boundaries [115]. The thermal history during forming processes can modify the grain size, making it susceptible to change. In the context of AM, the grain size of metallic materials differs from those of samples produced by casting [25], forging [116], or rolling [117] processes due to the unique thermal history involved.

Various methods have been employed to alter the grain size of AM-fabricated materials, as summarized in Table 2. Modifying grain and sub-microstructure sizes offers a feasible and promising approach to enhancing the HE resistance of AM-fabricated materials. Previous researchers have made attempts in this direction. For example, He et al. [123] investigated pure nickel printed via AM and observed that HE-induced cracks tended to propagate preferentially along the areas with fine grains in SSRT. As a result, the fabricated pure nickel sample with a 67° rotation angle for the successive printing layers exhibited a more tortuous fracture path due to its fine grain distribution. This sample demonstrated improved resistance to HE cracking compared to samples printed at 0° and 90° orientations (Fig. 8). Such findings suggest that manipulating grain distribution can be employed to enhance the HE resistance of AM-fabricated samples.

Table 2
Methods for controlling grain or sub-microstructure size of AM-fabricated samples.

Methods	Examples	Published by
Remelting	The grain size of Inconel 625 alloys fabricated using the LPBF technique was increased from 9 μm to 20, 21, and 27 μm through three different remelting parameters.	Ledwig et al. [118]
Adding reinforcement particles	The average grain size of LPBF-fabricated Al7075 alloy was decreased from 20.25 μm to 1.95 μm along the building direction by incorporating TiB_2 particles.	Liang et al. [119]
Heat treatment	The average grain size of AM-fabricated IN738 alloy decreased from 17.05 μm to 11.37 μm after stress-relief annealing at 600 °C for 24 h.	Zhang et al. [120]
Altering scanning strategies	A comparison study was conducted between samples fabricated with 0° and 90° rotation between successive layers. The result shows that the mean grain size of the 0° was ~80 μm, while that of 90° was ~139 μm.	Angelos et al. [121]
Altering printing parameters	Researchers increased the arm spacing of the dendritic structure in the X-Y plane of LPBF-fabricated Haynes 282 alloy from 0.4801 μm to 0.68 μm and the average grain size from 46.08 μm to 72.41 μm by increasing the energy density.	Boswell et al. [122]

Interestingly, the decrease in grain size has a controversial impact on the HE resistance in different studies. On the negative side, the grain size decrease can increase grain boundaries, providing more paths for hydrogen diffusion and trapping. This can accelerate the hydrogen diffusion process and the HEDE process during service, ultimately degrading the HE resistance of AM-fabricated materials [86]. For example, Wan et al. [44] compared the HE resistance of AlCoCrFeNi2.1 alloys formed by casting and the LENS method. They utilized the TDS method and found that the LENS-fabricated AlCoCrFeNi2.1 had higher hydrogen content due to the finer grain size and eutectic lamellae sub-microstructure compared to the wrought sample. Consequently, the elongation in SSRT for AM-fabricated AlCoCrFeNi2.1 (19.6%) was more impacted by HE than that of its wrought counterpart (48.5%). On the other hand, grain refinement may enhance the HE resistance of materials. Alnajjar et al. [124] found that larger grain size (~20.4 μm for LPBF after aging treatment and 9.1 μm for wrought after aging treatment) rendered higher HE sensitivity in LPBF-fabricated 17–4 PH stainless steel compared with its wrought counterpart in different SSRT tests; they proposed the coarser grain size of wrought 17-4 PH steel decreases the stresses needed for cracks initiation and propagation, resulting in the premature failure of LPBF-fabricated 17-4 PH steel in elastic domain. Neikter et al. [125] compared the HE resistance of EPBF-fabricated and casting Ti-6Al-4V alloys; they found that the fatigue crack growth rate under the hydrogen environment for the EPBF-fabricated samples is lower than that of the casting sample, and the presence of second cracks in EPBF samples (when stress intensity factor, ΔK up to 23 MPa $\sqrt{m}$) is later than that in casting samples (ΔK up to17 MPa $\sqrt{m}$). They attributed the improvement of HE resistance to the finer grain size and α laths sub-microstructure of EPBF-fabricated Ti-6Al-4V.

Based on the previous literature review in directly comparing the materials produced by conventional methods and AM, it can be seen that there is no consistent conclusion about which method can produce materials with better HE resistance or which grain size can facilitate better HE resistance. In the authors' opinion, those results suggest the presence of an optimal grain size for the HE resistance of additive manufactured materials. The infiltration of hydrogen can further diminish atomic bonding in this region, rendering grain boundaries brittle and expediting intergranular crack initiation or propagation, according to the HEDE mechanism. Since that, grain size refinement may augment overall hydrogen absorption, providing additional trap sites and transportation channels for hydrogen, while it concurrently diminishes the average hydrogen content per unit length of the boundary. Consequently, as pointed out by Zan et al. [126], optimal grain size is achieved when the hydrogen content per unit grain boundary length is minimized, which is not only a material-dependent factor but also strongly influenced by the charging method, time, and testing modes, in situ or ex situ. In addition, it is noteworthy that HE-induced transgranular fracture may also be accelerated along these brittle grain boundaries, further compromising the HE resistance of materials [127]. Regrettably, the prediction methods of hydrogen content per unit grain boundary length after the hydrogen charging process remain unclear. Although the intrinsic flexibility of AM methods presents considerable opportunities for grain size modification, a lack of clarity persists in predicting the hydrogen content per unit grain boundary length post-hydrogen charging. Further systematic investigative efforts are imperative to establish comprehensive guidelines or models capable of accurately predicting the impact of grain and sub-microstructure size on HE behavior across various materials and

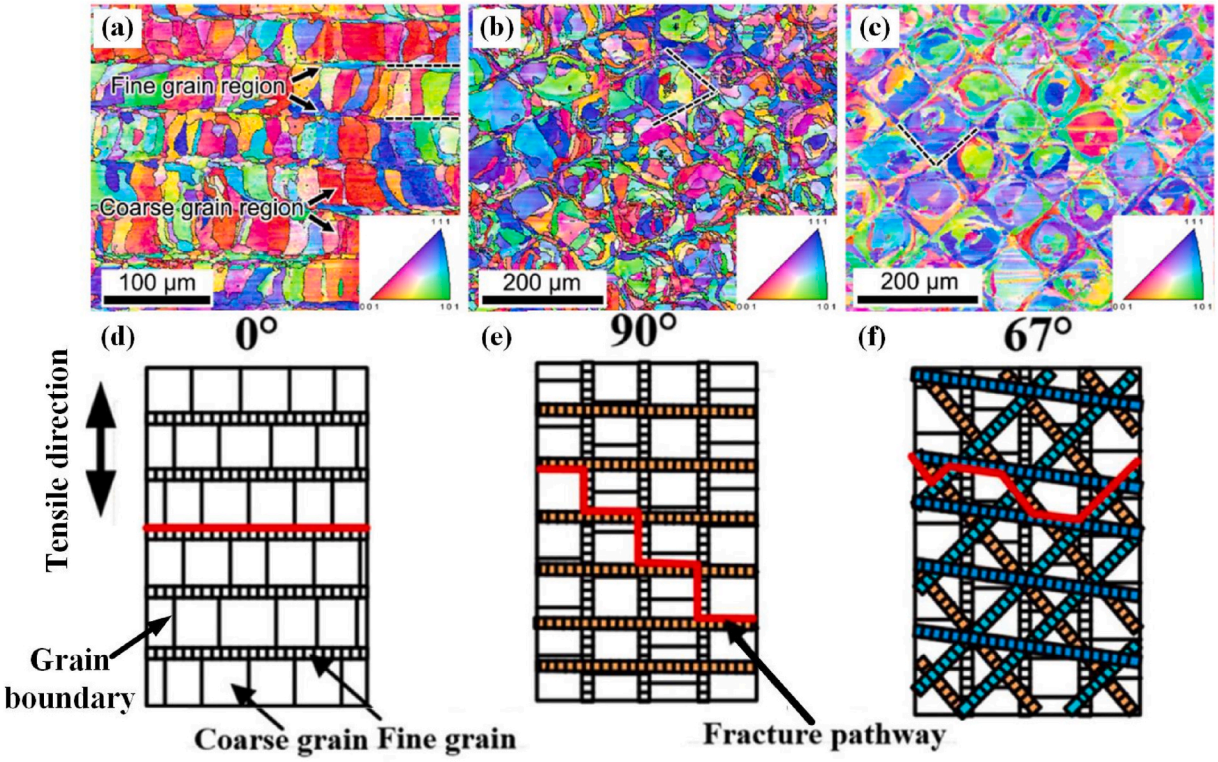

Fig. 8. Inverse pole figures and schematic of preferential fracture pathway for samples with rotation angle. (a, d) 0°, (b, e) 90°, (c, f) 67° [123].

manufacturing processes.

5.2. Dislocation density and morphology

As menthoed before, AM process usually exhibits much higher cooling rates, which are far beyond that of traditional methods. Associated with the elevated cooling rate during the AM process, dislocation cells, and high-density dislocation are more prevalent in AM-fabricated samples. This phenomenon significantly impacts the HE resistance of materials produced through AM. Various techniques have been employed to modify the dislocation density in metals, as summarized in Table 3, highlighting the feasibility of modifying dislocation density in AM processes.

Table 3
Methods for modifying dislocation density of AM-fabricated samples.

Methods	Examples	Published by
Heat treatment	Researchers studied LPBF-fabricated 316L stainless steel and observed a significant drop in the kernel angle misorientation (KAM) value from 0.99 to 0.16 after isothermal heating at 1200 °C for 2 h. The drop of KAM value suggests that isothermal heating can effectively decrease the dislocation density in the material.	Liu et al. [128]
Altering printing parameters	The geometric necessary dislocations (GND) density was increased from $1.9 \times 10^{15}\,mm^{-2}$ to $2.2 \times 10^{15}\,m^{-2}$ by decreasing the spot size of the electron beam and volume energy density in the EPBF process.	Sow et al. [129]
Laser shock peening (LSP)	Researchers investigated the effect of LSP treatment on the dislocation density of LPBF-fabricated Ti6Al4V alloy. Through TEM analysis, they observed an increase in the dislocation density in the treated samples. This rise in dislocation density corresponded to an increase in the hardness of the Ti6Al4V alloy, from 361 HV to 420 HV.	Guo et al. [130]

In general, the increase in dislocation density is detrimental to the HE resistance of AM-fabricated materials, based on the coupling effect of the HEDE and HELP mechanisms. The increased dislocation density can accelerate hydrogen transport, leading to the concentration of hydrogen in vulnerable sites such as grain and phase boundaries, resulting in premature fracture, according to the HEDE mechanism [88]. In addition, hydrogen is more efficiently transmitted by dislocations with higher density, accumulating particularly in dislocations proximal to crack tips experiencing stress concentration [88]. The resultant hydrogen accumulation intensifies the mobility of dislocations near crack tips, thereby expediting HELP-induced fractures [88]. This summary can be reflected in the study proposed by He et al. [131]. Their study involved a comparative analysis of LPBF-fabricated pure Ni samples with and without annealing. The research revealed that dislocation cells characterized by high dislocation density facilitate the transport of hydrogen into grain boundaries, inducing embrittlement and initiating cracks along these boundaries according to the HEDE mechanism. Then, the propagation process of those intergranular cracks was accelerated by the accumulation of hydrogen in dislocations near crack tips accelerates the HELP process, ultimately leading to premature fracture. The deleterious role of dislocations in impairing the HE resistance of materials is similarly evident in various studies, encompassing diverse materials such as CoCrFeMnNi high entropy alloy [132], 17-4 PH steel [133], and alloy 718 [134] fabricated by AM. On the other hand, dislocations can serve as pathways for the coalescence of voids; consequently, an escalation in dislocation density may expedite the HESIV process [94]. Despite this, little research within the realm of AM establishes a connection between the failure of hydrogen-charged samples and the HESIV mechanism, which should be further investigated by the following researchers.

However, in some other cases, the increase in dislocation density has a different impact on the HE resistance. Factors such as dislocation morphology [135] (e.g., the thickness of dislocation walls and dislocation tangles) and matrix properties [131] can strongly influence the impact of dislocation density on HE resistance. For instance, in a study

conducted by Zhou et al. [135], a positive influence of increased dislocation density on the HE susceptibility of LPBF-fabricated 304L stainless steel was observed. The study revealed that entangled dislocations served to impede the diffusion of hydrogen over large areas. The entangled dislocations consequently lead to a lower elongation loss but increased HE resistance in the as-received samples, compared with samples heat treated at 950 °C for 4 h (HT950-4). Their results are depicted in Fig. 9. This is due to the lower binding energy of hydrogen at dislocations compared to the activation energy in LPBF-fabricated 304L stainless steels with faced-central cubic steel, which impedes the diffusion of hydrogen and decelerates the HEDE process in vulnerable sites. On the contrary, steels with body-centered cubic structures have a higher binding energy of hydrogen at dislocations than activation energy [136].

Additionally, the entanglement of dislocations can enhance the ability of dislocations to trap hydrogen, further impeding the diffusion of hydrogen along dislocation channels. Interestingly, the interaction between hydrogen and dislocations in AM-fabricated materials can result in improvements rather than degradation in some cases. Bertsch et al. [137] observed that the elongation of annealed DED-fabricated 316L austenitic stainless steel improved by 7.02% after hydrogen charging, while the elongation of the as-fabricated counterpart decreased by 20.7% after charging. This improvement can be attributed to the ability of hydrogen to refine and stabilize the dislocation cell structures generated during the SSRT of the annealed samples. It is worth noting that this improvement is more commonly observed in samples with low initial dislocation density, particularly in annealed samples with lower dislocation density compared to as-fabricated parts, although the precise mechanism behind this phenomenon is not yet fully understood.

Currently, the influence of dislocation density on HE resistance for AM-fabricated materials remains inadequately understood among researchers, particularly concerning the underlying mechanisms governing hydrogen transportation and the trapping process at dislocations. Furthermore, few researchers have focused on precisely predicting the relationship between hydrogen binding and trapping ability of dislocations and dislocation morphology of materials, areas that require further attention in future research endeavors.

5.3. Molten pools

In various metallic AM methods such as LPBF, DED, and EPBF, molten pools are a common microstructural feature. During these processes, metallic powders are rapidly melted into a liquid state, followed by shrinkage due to surface tension forces, and eventually solidification, forming semi-arc MPB. Liu et al. [138] investigated the electrochemical performance of MPB in LPBF-fabricated 316L steel during the hydrogen charging process. They found the dramatic thermal fluctuation process leads to the element partition, resulting in the aggregation of hydrogen along MPB. This hydrogen concentration enhances the susceptibility to cracking in the MPB area, thus initiating HE-induced cracks and their propagation from this region, as depicted in Fig. 10.

However, a more comprehensive investigation into the effect of the MPB is warranted and should be pursued by researchers. In general, the sub-microstructure within or near the MPB area tends to be coarser compared to the microstructure within the molten pool. This difference in the sub-microstructure may influence the rate of hydrogen diffusion. In addition, the sharp angle area (shown in Fig. 11a by a red circle and arrows) is subjected to stress concentration in the AM process because it is a junction site for different molten pools. The cooling process and associated shrinkage in this area can lead to the accumulation of residual stresses and concentrations [140]. Additionally, the sub-microstructure orientations on both sides of the sharp angle area can be significantly different due to the influence of the thermal gradient, as illustrated in Fig. 11b [139]. Therefore, cracks are more likely to initiate from the sharp angle area during SSRT due to these factors. However, only limited research has focused on these specific issues, indicating the need for further investigation in future studies.

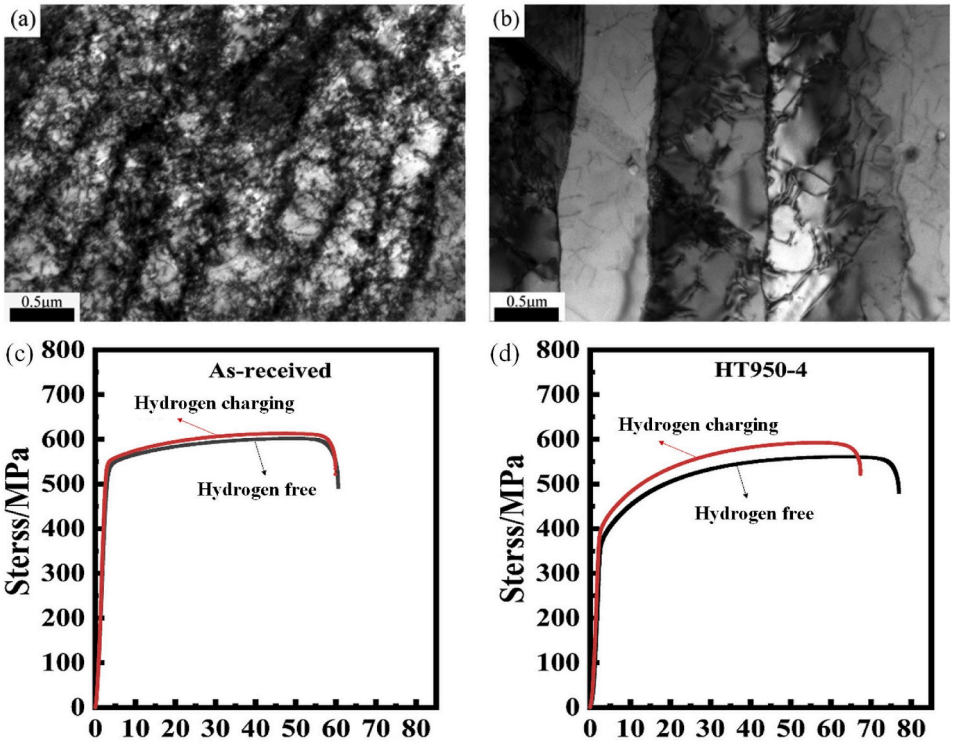

Fig. 9. TEM images of (a) as-received ed 304 sample with entangled dislocations, (b) HT950-4, engineering stress-strain curves with and without hydrogen charging for (c) as-received sample, (d) HT950-4 sample [135].

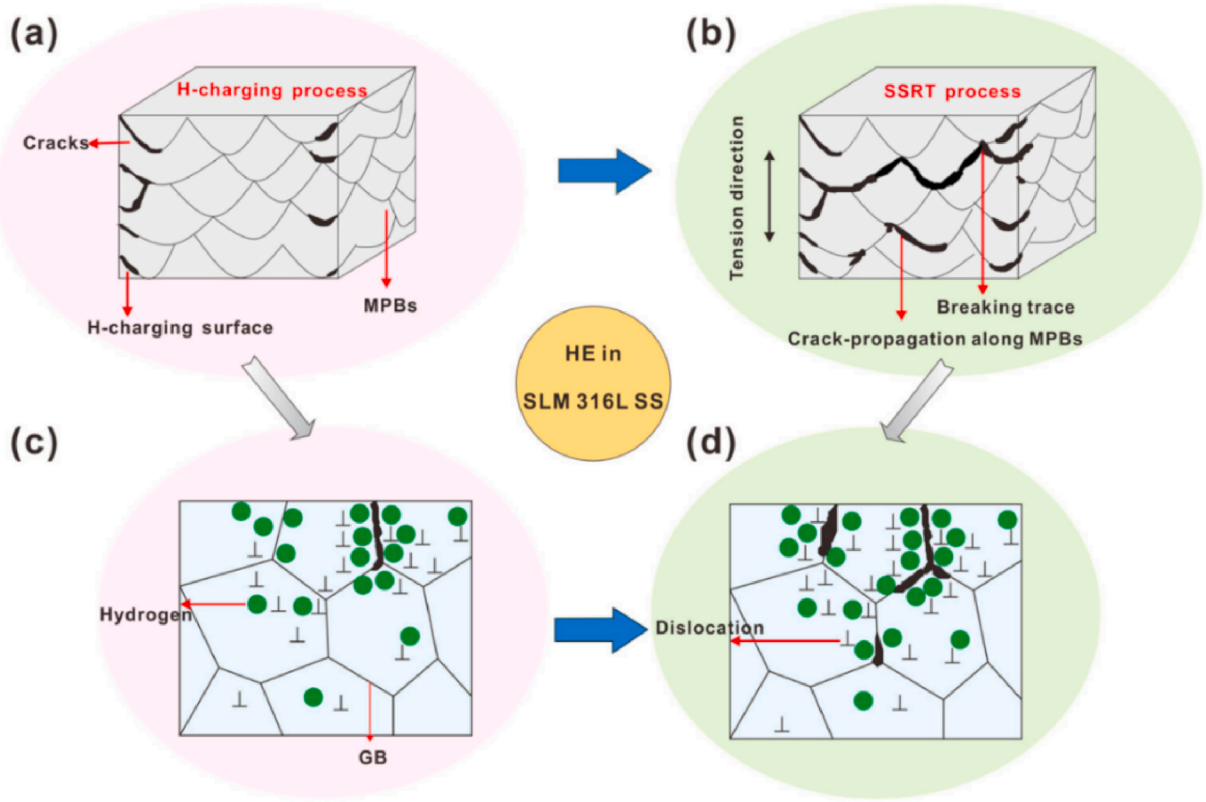

Fig. 10. Schematic diagram of HE processes in SLM 316L stainless steel. (a, c) hydrogen enrichment and crack initiation in the MPB area during the hydrogen charging, (b,d) crack propagation process in SSRT along MPB [138].

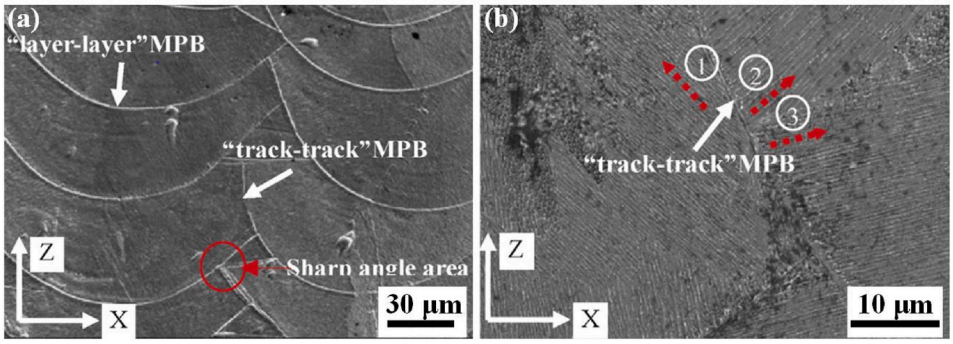

Fig. 11. Morphology of molten pool and its boundaries. (a) low magnification image (b) Partial enlargement image of sharp angle area [139].

5.4. Secondary phases

Secondary phases in AM-fabricated materials originate from two primary sources.

1. Introduced reinforcement particles: this is a common approach to enhance the service properties of components. For instance, Han et al. [141] successfully eliminated cracks in LPBF-fabricated Hastelloy X alloy by incorporating TiC particles, which prevented premature fracture in high-temperature working environments.
2. Precipitated phases: secondary phases can precipitate from the matrix during the AM process or heat treatment, such as the generation of $M_{23}C_6$ carbides in LPBF-fabricated Hastelloy X alloy [25].

In general, secondary phases tend to increase the HE susceptibility of AM-fabricated materials in most cases. This is primarily because secondary phases can serve as irreversible trap sites for hydrogen absorption [142]. Moreover, the interfaces between the secondary phases and the matrix can act as fast diffusible paths for hydrogen [143]. Consequently, the edges of secondary phases are prone to hydrogen concentration, initiating crack formation based on the HELP and HEDE mechanisms. Fig. 12 illustrates this phenomenon. In certain instances, hydrides may distribute along grain boundaries or sub-microstructure boundaries with low cracking resistance, leading to intergranular cracking. Yoo et al. [134] found that the distribution of the δ phase along grain boundaries increased the hydrogen content in those regions, resulting in the initiation of cracks and voids and accelerating the fracture of LPBF-fabricated Nickel-based 718 alloy during SSRT. Xu et al. [144] similarly observed that γ′ and γ" precipitates formed along the boundaries of cellular structures after heat treatment, enhancing the HE susceptibility of LPBF-fabricated 718 alloy.

Besides, secondary phases can also form during the hydrogen charging process. For example, Kong et al. [145] observed the presence of δ-TiH_X hydrides in heat-treated LPBF-fabricated Ti6Al4V alloy after

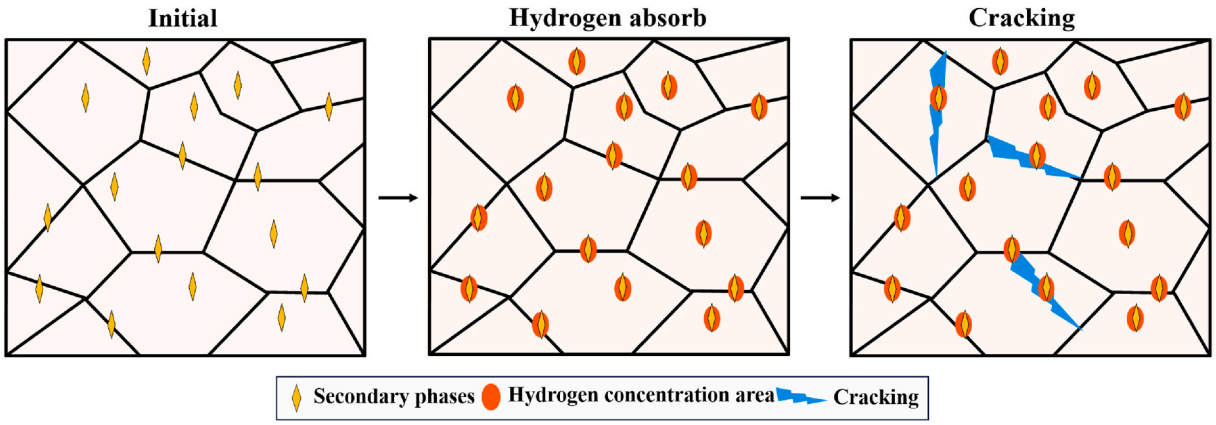

Fig. 12. Schematic diagram for hydrogen-induced cracking caused by secondary phases.

hydrogen charging. These brittle hydrides dispersed along the interface of α/β phases, transforming the fracture behavior from ductile to brittle. It is worth noting that the occurrence of brittle hydrides is quite common since δ-TiH_X forms from the Ti-based matrix when the hydrogen concentration exceeds the solubility limit [146]. This aspect should be taken into consideration in investigations involving Ti-based alloys. Although the impact of low content of secondary phases on HE resistance may not be significant in certain studies [136,137,147], it is still an aspect that researchers should focus on.

5.5. Defects

Defects in AM-fabricated materials have a detrimental effect on their HE resistance. According to the hydrogen molecule recombination mechanism, defects can offer cavities for H_2 recombination and increase the air pressure within defects [80]. For example, H_2 is found in the cavities of droplets fabricated by underwater WAAM, making them more prone to breaking [80]. Defects can also act as sites for crack initiation or growth, accelerating the fracture process under a hydrogen environment [148], because stress concentration at the edges of defects leads to hydrogen accumulation [149]. Liesbet et al. [150] observed hydrogen near the porosity in LPBF-fabricated Ti6Al4V samples after SSRT, indicating hydrogen concentration in that area.

Defects in AM-fabricated samples are common due to the intense temperature changes during the AM process. They can be categorized into two types.

1. Porosity: massive porosity is typically attributed to unsuitable volume energy density (VED) caused by inappropriate printing parameters [151], which is common in PBF and DED. Intense matrix evaporation can occur when the VED is too high. As a result, gas may be trapped by the viscous liquid of the molten pool, forming gas pores with nearly spherical shapes after cooling. Conversely, if the VED is too low, metallic powders may not fully be fused, leading to irregular unmolten voids in the material [152]. The porosity rate significantly affects the HE resistance of AM-fabricated materials. However, limited research has investigated the effect of porosity variation caused by process parameters on the HE resistance, or its impact may be overshadowed by other factors due to the high density of AM-fabricated materials [144,148,150].
2. Microcracks: various factors can lead to cracking in AM-fabricated samples, including intense residual stress accumulated during the AM process [153], deteriorated precipitation [154], and low melting point eutectic liquid films [141]. Moreover, as-built AM specimens often exhibit elevated surface roughness, leading to higher crack density in both the surface and subsurface regions. This phenomenon can be attributed to the characteristic staircase effect inherent in the AM process [150]. In addition to the degradation mechanisms common to defects, pre-existing cracks can serve as preferential sites for fracture under the influence of the HELP mechanism (as discussed in Section 4.1). For instance, Neikter et al. [125] conducted fatigue tests on EPBF-fabricated Ti6Al4V in high-pressure H_2 and dry-air environments. They observed that the crack growth rate in the hydrogen environment quickly exceeded that in the dry air environment when the cycles exceeded approximately 6000 cycles, indicating that hydrogen diffusion can accelerate crack propagation and degrade the HE resistance of the material.

To eliminate defects in AM materials, Feng et al. [155] applied the HIP for LPBF-fabricated CoCrFeNiMn high-entropy alloys; HIP can decrease the number of microcracks and micropores, and relieve the residual stresses (from 338 ± 4 MPa to 44 ± 4 MPa) inner printed sample, which is beneficial to prevent the growth and initiation of crack. Thus, the elongation loss of the charged samples decreases from 80% to 61.4% after HIP. Other methods, such as LSP [156], and the addition of reinforcement particles [157], have also been found to be effective in eliminating defects.

5.6. Grain crystallographic and spatial orientation

For materials fabricated by PBF and DED, the grain crystallographic orientation is $<001>$ (along the building direction) in most cases, and an elongated grain morphology along the building direction in terms of the grain spacial orientation [158,159]. The melting and remelting process during AM stimulates preferential grain growth. This preferential grain crystallographic and spacial orientation can result in differences in microstructure on different planes, thereby influencing the HE resistance of materials and causing anisotropy in HE performance. While the investigation of the effect of the grain crystallographic orientation on HE susceptibility remains a blank area, several studies focused on the effects of grain spatial orientation.

Hesketh et al. [147] pointed out that HE-induced cracks are more prone to propagate along the grain orientation when the hydrogen charging orientation is parallel to the grain orientation in AM-fabricated components using a sulfuric acid solution (Fig. 13). The preferential grain growth also leads to flat grain boundaries along the grain orientation, providing pathways for hydrogen diffusion and crack growth. Their research showed higher elongation loss (77%) for horizontally built samples in the hydrogen environment compared to the wrought counterpart (58%). Conversely, when the hydrogen charging orientation is perpendicular to the grain orientation, rugged grain boundaries relieve hydrogen diffusion and crack propagation, resulting in lower elongation loss for vertically built samples (37%) compared to the wrought counterpart. Similar results were observed by Deconinck et al. [150] and Wu et al. [160], indicating better HE resistance of vertically built LPBF-fabricated Ti6Al4V than the horizontally built counterpart in

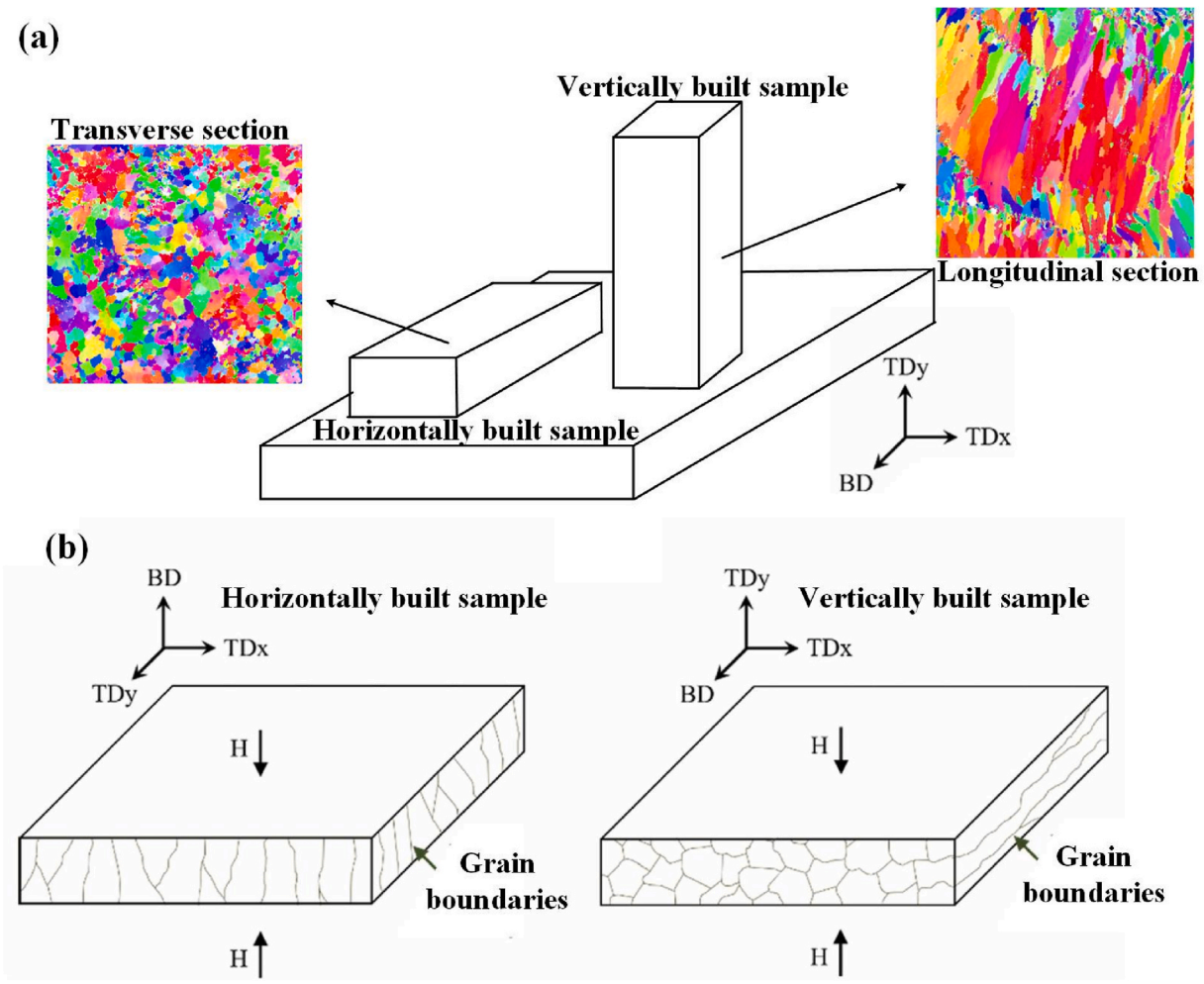

Fig. 13. Schematic diagram of hydrogen diffusivity in horizontally and vertically printed samples. (a) Microstructure of the transverse section and longitudinal section for horizontally and vertically built samples (EBSD images from unpublished work of authors), (b) schematic diagram for the relationship of hydrogen diffusion and grain orientation [150].

a liquid environment.

Interestingly, Silverstein and Eliezer [161] found that the HE resistance of horizontally built Ti6Al4V was better than that of the vertically built counterpart in a high-temperature gas environment. This may be attributed to the better penetration of high-temperature hydrogen gas and the lower total length of prior β grain boundaries in the horizontally built Ti6Al4V [150]. The former factor weakens the influence of grain orientation on HE resistance, while the latter reduces the speed of hydrogen diffusion. This result suggests that the impact of grain spatial orientation can be affected by the state of hydrogenation, although the exact mechanism is not yet clear.

6. Effect of processing methods and parameters on the HE resistance

6.1. AM processing parameters

As discussed in Chapter 5, variations in printing parameters result in changes to the microstructure, including grain size, dislocation density, and defect distribution. These changes occur because alterations in printing parameters significantly influence the thermal distribution and solidification process of the material, which in turn impacts the HE resistance. This provides a feasible strategy for mitigating HE. For instance, Cheng et al. [148] compared the hydrogen-induced elongation loss of LPBF-fabricated high-entropy CoCrFeNiMn alloys printed with different VED (71.43, 81.02, and 90.23 J/mm^3). They found that at a VED of 81.02 J/mm^3, the CoCrFeNiMn alloy exhibited the highest HE resistance, with only a 0.4% elongation loss. In contrast, inappropriate VED values resulted in the formation of microcracks, which act as potential initiation sites for cracking during the hydrogen charging process, thereby reducing the alloy's HE resistance. However, it is important to note that variations in printing parameters simultaneously affect multiple microstructural features. Further research is required to understand how these microstructural changes interact, in order to optimize printing parameters for enhanced HE resistance.

6.2. Manufacturing methods

It is a central interest to benchmark the HE performance of the same alloys manufactured via AM and conventional methods. Table 4 summarizes the comparative studies in the literature with different alloy systems. In general, AM-fabricated and conventionally fabricated samples consist primarily of similar phases when produced from materials with the same chemical composition. However, the AM process typically exhibits much higher cooling rates compared to traditional fabrication methods. As a result, AM-fabricated samples generally have smaller grain sizes and higher dislocation densities, which significantly influence their HE resistance. The generation of MPBs during AM processing also negatively impacts the HE resistance of materials.

Furthermore, the effects of AM methods on hydrogen behavior are

Table 4
Comparison for the HE resistance of conventionally and AM-fabricated samples.

Alloying system	Materials and fabrication methods	Performance	Underlying mechanism	References
High entropy alloy	AlCoCrFeNi2.1 casting vs. LENS (AM)	7% UTS loss for the casting sample caused by HE, while 5% UTS loss for the LENS-fabricated sample.	The finer grain size of LENS-fabricated AlCoCrFeNi2.1 leads to higher hydrogen uptake compared with casting counterparts, which aggravated the HEDE and HELP-induced degradation.	Wan et al. [44]
Ti-based alloy	Ti-6Al-4V alloys casting vs. EPBF	AM supiror (delayed fatigue cracking)	Finer grain size and α laths sub-microstructure in AM microstructure delay fatigue crack initiation.	Neikter et al. [125]
Fe-based (Martensite)	17-4 PH steel wrought vs. LPBF	Conventional supiror under different strain rates and charging conditions.	Cracking is more easily initiated and propagated in LPBF-fabricated stainless steel with reduced grain size.	Michella et al. [124]
Fe-based (Austenite)	304L stainless steel forging vs. LPBF	AM superior (less ductility loss)	Cellular structures by AM can trap hydrogen and impede hydrogen accumulation in grain boundaries, alleviating the hydrogen-induced cracking in grain boundaries.	Zhao et al. [162]
Fe-based (Austenite)	304L stainless steel casting vs. LPBF	AM superior (after 1 day and 5 days of hydrogen charging, LPBF-fabricated samples exhibited 7% and 19% elongation loss, respectively. While the casting counterparts show 28% and 55% elongation loss, respectively.)	Cellular structures and more homogeneous element distribution in AM materials help suppress the formation of α′ martensite in the tensile process. The area of α′ martensite would be the preferential site for crack initiation, which degrades the HE resistance of casting counterparts.	Lee et al. [136]
Fe-based (Austenite)	Low carbon ferritic steel Fe-(1.8-2.1)Mn-(0.7-1.0)Si-(0.05-0.11) C casting vs. EBAM	AM superior (less elongation loss)	AM process reduces pearlite phase and carbon content in the matrix, lowering susceptibility.	Panchenko et al. [163]
Ni-based alloy	Inconel 718 wrought vs. LPBF	AM superior (less elongation loss)	The presence of γ′ and γ″ phase aggravated HE in wrought sample	Monhands et al. [164]

also reflected in increased residual stresses. Deconinck et al. [150] suggested that intense residual stresses are a key factor that promotes hydrogen absorption, thereby decreasing the HE resistance of LPBF-fabricated Ti-6Al-4V. These residual stresses can cause matrix distortion [165], leading to hydrogen accumulation and accelerating crack initiation or propagation due to hydrogen-induced embrittlement. This hypothesis was supported by Nishimura et al. [166], who found that after hydrogen charging of stretched-formed tempered martensitic steel sheets, cracks initiated from regions with the highest residual tensile stress. Due to the repeated expansion and shrinkage caused by rapid melting and solidification, the residual stresses in AM-fabricated samples are typically much higher than in traditionally fabricated counterparts [165]. Although residual stresses can be alleviated through heat treatment, this process increases production costs and poses challenges for large-scale components.

In addition, HE resistance can be influenced by the choice of AM fabrication methods. As mentioned in Chapter 2, PBF and DED are two primary fabrication methods for components exposed to hydrogen environments. Compared to PBF, DED generally uses larger powder particles, with an average diameter exceeding 50 μm [167]). This is because smaller particles have higher surface energy [168], which makes them more likely to aggregate and block the deposition head's channel [169]. Moreover, in wire-fed DED, the control of material input is affected by the cross-sectional area of the wire. Consequently, DED-fabricated samples typically exhibit higher surface roughness than PBF-fabricated samples. Deconinck et al. observed that, when comparing LPBF-fabricated Ti-6Al-4V before and after machining, the as-fabricated Ti-6Al-4V with higher surface roughness demonstrated poorer HE resistance because the rough surface increased the effective surface area available for hydrogen absorption [150], as shown in Fig. 14. Based on this, it can be inferred that DED-fabricated samples may exhibit lower HE resistance than PBF-fabricated samples. However, this hypothesis has not yet been fully substantiated by published research. Besides roughness effects, further research is also needed to compare the effect of differences in microstructure features caused by different AM methods to the HE resistance.

6.3. Thermal processing

As a widely used thermal processing method, heat treatment can significantly influence the grain size and dislocation density, leading to the optimization of material microstructure and improved resistance to hydrogen embrittlement. In addition, heat treatment can effectively reduce the accumulation of residual stresses and microdefects in samples, thus increasing their HE resistance. For instance, Zhao et al. [170] reduced the elongation loss from 92% to 0% through solution treatment of AM-fabricated 18Ni300 samples charged at a hydrogen current density of 0.05 mA/cm^2. Except for heat treatment, emerging thermal processing techniques like in-situ remelting have shown promise in altering grain size and dislocation density, as mentioned in Table 2andTable 3. During the in-situ remelting method, printed layers are remelted with an additional laser during the printing process, thereby impacting the thermal history of the material. Another promising technique is the control of pausing time. Philipp et al. [171] applied temporary pausing in the DED process and found temporary pausing can modify the thermal history of printed materials, enabling the generation of beneficial precipitates like $(Ni, Fe)_3$. Given the thermal history can also affect the microstructure (e.g. grain size and dislocation density), adjusting the pausing time could be a potential way to optimize the HE resistance of the material.

6.4. In-situ additional physics treatments

Utilizing additional in-situ physical treatments has emerged as a significant strategy for researchers aiming to enhance the HE resistance of metals. Inspired by the casting process, Todaro et al. [172] applied

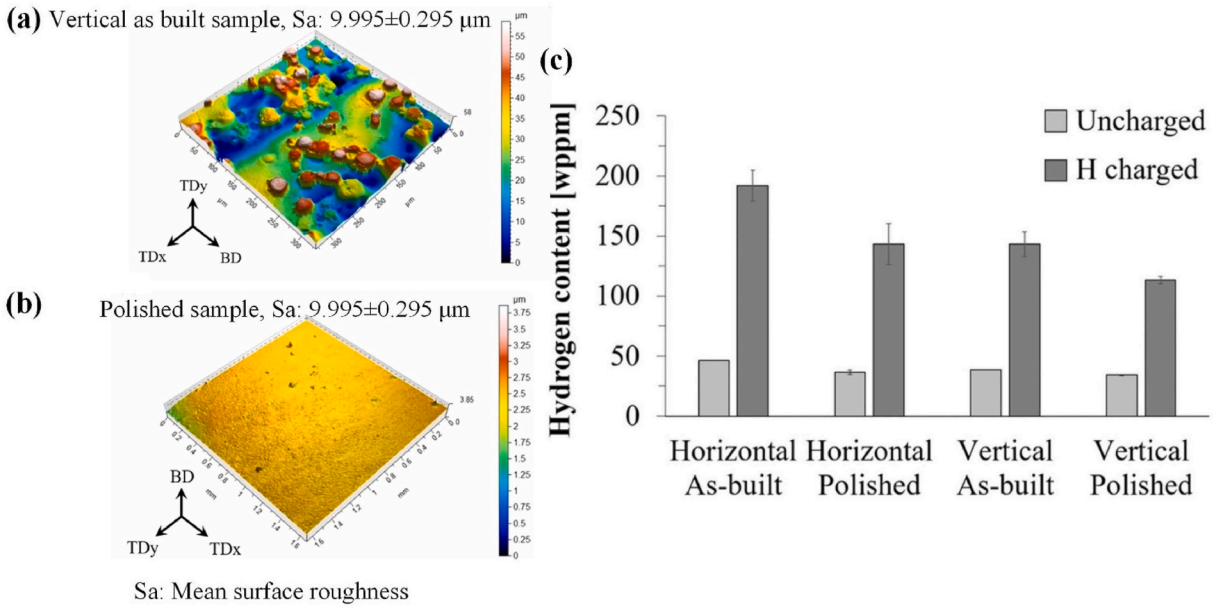

Fig. 14. Surface roughness of (a) vertical as built sample, (b) polished sample, (c) Hydrogen content of polished and unpolished sample after hydrogen charging [150].

(high-intensity ultrasound) HIU during the DED process. This method promotes grain refinement (from 500 μm to 117 μm) by creating numerous cavitations for nucleation sites in the molten pool. As mentioned in Section 5.1, grain refinement is helpful in modifying material into optimal grain size for HE resistance. However, its full potential remains untapped. Molten pool vibration may mitigate element segregation and decrease detrimental phase content, thus alleviating the hydrogen accumulation in the molten pool and detrimental phases, and the detailed mechanism has been elaborated in Section 5.3 and Section 5.4. Despite this, little research focuses on the function of HIU in HE mitigation. The LSP method is another underlying in-situ additional physics treatment method. LSP involves transmitting a pulsed, focused laser beam through a water-confining layer to impact the surface of as-built layers. As indicated in Table 3, LSP significantly increases sample dislocation density, thereby reducing hydrogen transportation. Additionally, LSP induces compressive stresses and thus closes microcracks generated [156] during manufacturing, offering the potential to enhance HE resistance in cracked samples. As explained in Section 5.5, the removal of cracks can increase the HE resistance of the material. This characteristic of LSP may provide a new way to improve the HE resistance of cracked samples.

7. Current challenges and future opportunities

7.1. Large-scale components

The demand for AM-fabricated large-scale components emerges with the development of technology [173]. Currently, AM-printed components can exceed 5 m in height and length using the DED method without a vacuum chamber [174]. However, when considering printers with vacuum chambers, Sciaky company claims to have developed the EBAM 300 Series, which is touted as "the largest 3D printer in the world, " with a building envelope of up to 6.10 × 1.40 × 1.37 m [175]. It is important to note that the EBAM 300 Series requires a large vacuum chamber with dimensions of 7.62 × 2.74 × 3.35 m, resulting in significant gas wastage, increased machine cost, and higher material consumption. Therefore, from an economic standpoint, fabricating large-scale components in an open-air environment is more practical than within a closed vacuum environment. In some cases, the repair of large workpieces needs to be conducted in an open-air environment.

However, printing components in the open-air environment inevitably exposes the large-scale components to external hydrogen during the AM process. Although the application of protective air can mitigate hydrogen ingress into the molten pool, it does not completely prevent hydrogen entry into the molten pool or the fabricated portion with high residual thermal energy [176,177]. For example, Elmer et al. [178] fabricated pure tantalum samples via WAAM and protected the molten pool using high-purity argon torch shielding gas under an air atmosphere; they found that the hydrogen content in the as-fabricated tantalum sample was 7.64 ml/100 g, significantly higher than that in the wire arc (1.35 ml/100 g). The absorption of hydrogen in the forming process may result in hydrogen-induced cracks [179], pores [79], and hybrids in as-fabricated samples before service, which leads to the presence of substandard workpieces. In the case of large-scale components, the voluminous size amplifies the consequences and economic losses in the event of failure due to HE. In addition, residual thermal stresses are more subject to accumulating in bulky samples than in small samples [180]. The accumulation of residual stresses can accelerate the generation of cracks, thus degrading the HE resistance of components [181]. To solve this problem, Derekar et al. [182] applied a cold metal transfer technique to reduce the energy input in the WAAM process. This decrease in energy input reduced the thermal residual stresses and hydrogen absorption, consequently lowering the porosity rate of the sample from 0.106% to 0.05%. Nevertheless, the impact of HE on large-scale AM-fabricated samples has not received sufficient attention from the academic community. It is expected to become a significant obstacle in the fabrication of bulky metallic workpieces in the future.

7.2. Energy industry

Currently, the full potential of AM in the energy industry remains largely untapped, primarily due to uncertainties surrounding the long-term in-service properties of AM-fabricated components, particularly their resistance to HE. Unfortunately, the utilization of AM in the energy industry is rare, with most applications still in the planning stages. Given that energy industry components (as shown in Table 5) often come into contact with high-temperature steam, natural gas, hydrogen gas, fuel oil, or LH. The possibility of unpredictable HE-induced fractures poses a significant risk of causing casualties and severe contamination in the energy industry. Consequently, engineers exercise caution when

Table 5
Components and corresponding materials serving in the hydrogen environment.

Components	Materials	Components	Materials
Boiler tubes of power plants 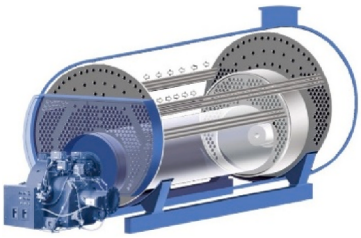 (Attributor: Pourabdollah et al. [183])	St.20 steel [184].	High-pressure natural gas cylinders  (Attributor: Arens et al. [185])	Austenitic stainless steel (like AISI 316 and 304 and AISI 316L and 304L [98].
Valve 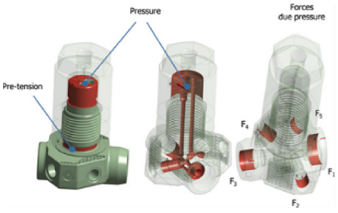 (Attributor: Kedziora and Cao [186])	AISI 4340 for hydrogen storage [186], 17-4 PH stainless steel for gas plant [187]	Nuclear reactor 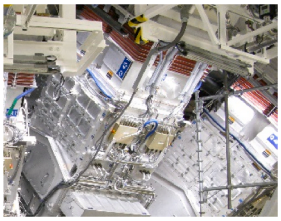 (Attributor: Steve Jurvetson)	Nickel-based Alloy 600 [188].

considering the application of AM technology, resulting in a slower adoption rate compared to the aerospace industry [47].

Nevertheless, the significant application potential of AM in the energy sector can be deduced from the emergence of ambitious application plans. For instance, GE has predicted a potential income of 2 billion dollars from the application of AM in oil and gas exploration and transportation facilities [47]. GE has also initiated testing of AM-fabricated components, including centrifugal pumps and turbines [189]. In the realm of nuclear plant facilities, Westinghouse has successfully printed a metallic thimble plug weighing 600 kg for practical application in a nuclear reactor, with plans to produce more in the future [190]. In summary, the demand for the application of AM technology in the energy industry is steadily increasing.

The merits of AM exhibit commonalities across various branches of the energy industry. To provide an insightful perspective, this article will discuss the potential applications of AM in H_2 storage and transportation, an area that has received limited attention in research orientation. Currently, two primary mechanical methods for H_2 storage are high-pressure gas storage [191] (fit for 800 bar) and cryogenic LH storage (holding at 21.15 K) [192]. However, the storage environment for H_2 presents significant challenges for containment materials. Prolonged contact with gaseous or liquid hydrogen leads to additional issues in metallic containers. Hydrogen gradually permeates the surface of the vessel, forming bubbles that result in material embrittlement and

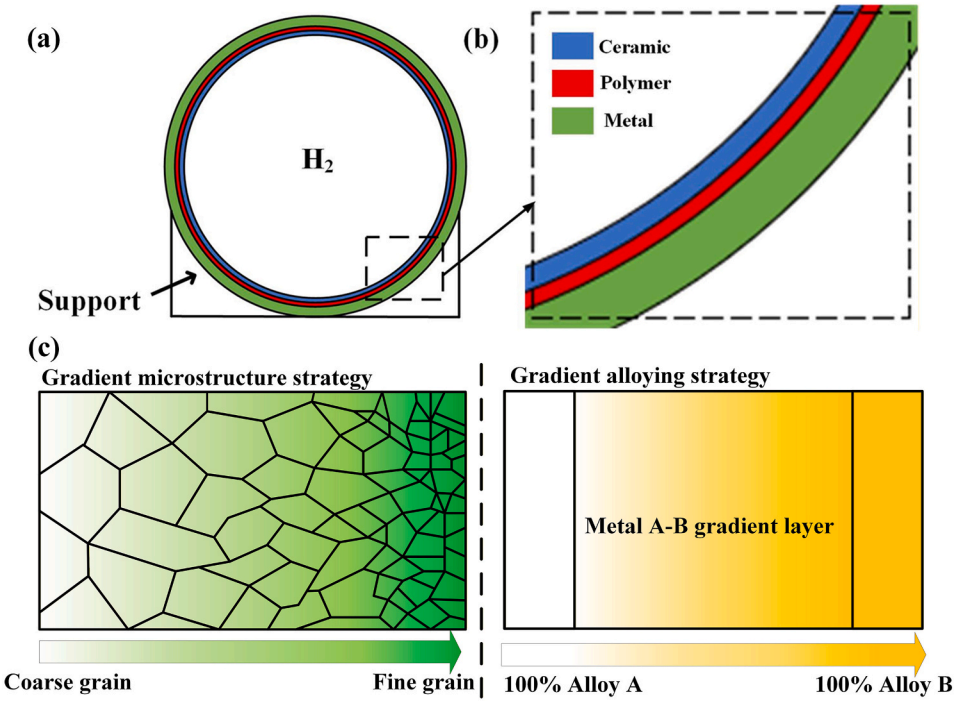

Fig. 15. Design of triple-layer H_2 containers. (a) Overall map, (b) partial enlargement map, (c) Gradient strategies for the MMAM fabricated metallic materials.

structural failure [193]. Polymer materials possess improved resistance to embrittlement, but their strength is not ideal for service applications [191]. Ceramics demonstrate excellent low- and high-temperature resistance; however, they tend to be porous and brittle [194].

To address these challenges, the authors propose a triple-layer design, as illustrated in Fig. 15. The inner side of the containers would incorporate a ceramic layer to prevent the cryogenic or high-temperature H_2 gas from reaching other components. A medium polymer layer would serve as a barrier, preventing H_2 entry through the porous ceramic and into the metallic shell. The outer metallic parts, known for their strength and ductility, would protect against external impacts or vibrations caused by the natural environment. When employing conventional fabrication methods (e.g., vapor deposition method and centrifugal casting method), the production of composite materials is often a time-consuming process [195]. In addition, traditional approaches tend to result in lower surface quality and bonding strength among different layers [196]. This is primarily due to the varied thermal expansion efficiency of the distinct layers involved in the composite material [197]. Nevertheless, it can be accomplished using upgraded AM machines with MMAM capabilities. For example, Han et al. [198] developed a projection micro-stereolithography with dynamic fluidic control, enabling the printing of polymer, ceramic, and metal as a single integrated structure. Zhang et al. [197] also upgraded their LPBF machine to incorporate MMAM functionality. Another storage option, the chemical storage method, can also benefit from MMAM. H_2 absorption materials (e.g., $MgH_2/Mg(NH_2)_2$ hydride [199] and nanostructure carbon [200]) can be deposited on the surface of the metal using MMAM, reducing material costs while increasing the contact area between H_2 and absorption materials.

To leverage the design freedom of AM for enhancing HE resistance, two gradient material strategies are proposed in Fig. 15c. The objective is to achieve an optimal combination of HE resistance, structural integrity, and cost-effectiveness. 1. Gradient microstructure strategy: Based on a single alloy system, this approach tailors local features. An HE-resistant microstructure is fabricated on the hydrogen-contact surface, transitioning to a core structure optimized for strength or ductility. A prime example is grain size engineering. as shown in Fig. 15c, a fine-grained outer layer is deposited to maximize HE resistance via the dilution effect when the hydrogen conventionally is rather low. This gradually transitions to a coarse-grained core to ensure superior bulk ductility. 2. Gradient alloying strategy: This multi-alloy approach places alloy B, characterized by a low hydrogen diffusion coefficient but lower strength (e.g., Al alloys or 316L stainless steel), on the hydrogen-contact surface. Simultaneously, a stronger alloy A (e.g., martensitic steel) is utilized in the core to provide structural reinforcement or reduce costs. A graded transition layer, consisting of tailored proportions of alloys A and B, is introduced to ensure metallurgical compatibility and structural continuity between the distinct regions.

Moreover, the layer-by-layer fabrication characteristic of AM offers significant advantages for the advancement of H_2 processing and storage equipment and components. It enables the implementation of in-situ monitoring during the manufacturing process [201], which is instrumental in reducing the porosity rate and enhancing the air-tightness of H_2 containers. Furthermore, this characterization substantially enhances the design flexibility of AM machines, thereby reducing the processing time and cost associated with manufacturing components for H_2 containers and processing machines with intricate structures, such as valves. In conclusion, it can be anticipated that AM technology will progressively gain prominence in the energy industry, proving to be valuable in the years to come.

7.3. Underlying HE mechanisms

The complexity of HE phenomena in AM fabricated materials has been fully elaborated in Chapters 4 and 5. A summary is provided here from different length scales, as depicted in Fig. 16. Due to the additional extrinsic and intrinsic features brought by the AM processes, the HE mechanisms and the triggering features are more complex than those of materials by conventional fabrication methods. Therefore, the following three scales are distinguished.

1. Mesco-scale

Reducing the surface roughness is the main challenge in HE resistance ability at the mesoscale level. Rough surfaces often harbor cracks, providing paths for hydrogen atoms to get in. Conventional surface treatment methods such as cutting [202], pickling [203], and laser remelting [204] can be applied to AM-fabricated samples to smooth surfaces. However, further research is encouraged on their impact on HE resistance.

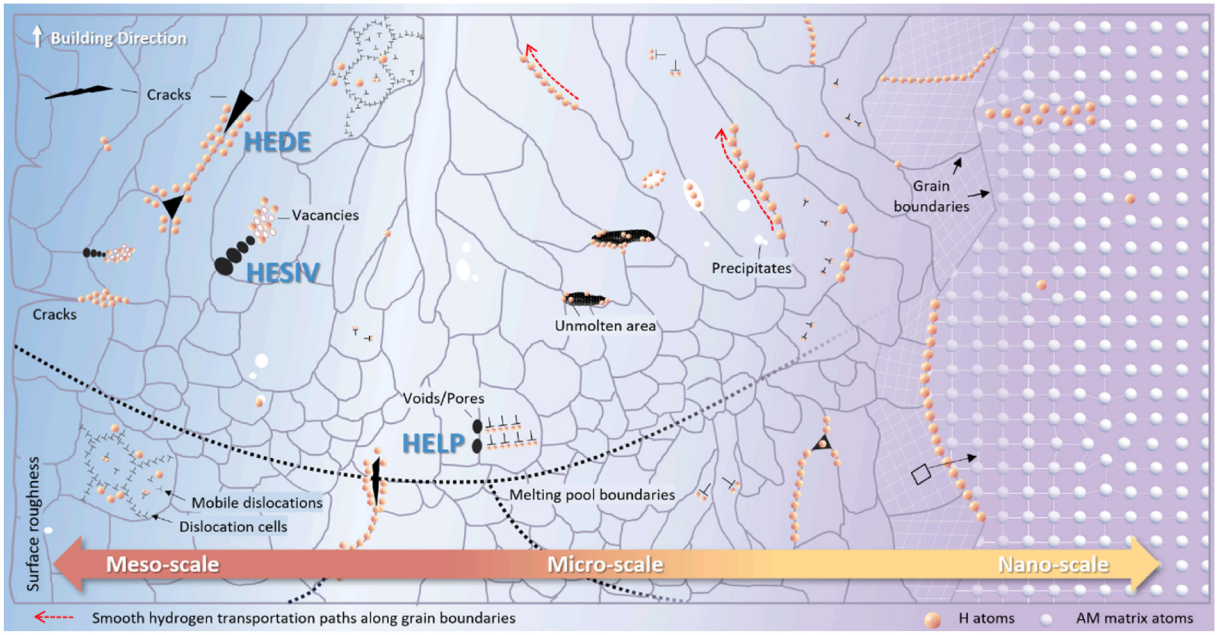

Fig. 16. Schematic diagram of hydrogen embrittlement in AM-fabricated metals.

2. Micro-scale

Hydrogen accumulation within AM-fabricated samples occurs at various microstructural sites, primarily occupying interstitial spaces, grain boundaries, vacancies, and dislocation cores. Additionally, the unique nature of AM introduces specific accumulation sites such as MPBs and segregated precipitates. This local concentration accelerates the HEDE process, a mechanism often facilitated by efficient transport channels, specifically, the smooth, continuous grain boundaries of columnar grains aligned with the building direction. Moreover, this hydrogen accumulation may increase the dislocation mobility, and expedite crack propagation, ultimately leading to sample fracture, as proposed by the HELP theory.

However, the influence of grain size and dislocation density on HE resistance remains controversial. A 'double-sided' effect is observed regarding grain size: on one hand, grain refinement creates a 'dilution effect,' increasing the total grain boundary area to distribute hydrogen and keep local concentrations below the critical threshold for HEDE. On the other hand, finer grains can increase the total hydrogen 'uptake,' as the dense network of boundaries facilitates absorption and trapping, eventually leading to embrittlement once saturation is reached. This reveals that HE resistance is not solely determined by intrinsic microstructure but is also highly dependent on extrinsic factors, such as hydrogen concentration and charging conditions. Higher concentration and active charging will facilitate the absorption function of the fine grain, detrimental to HE resistance, while a lower concentration of hydroben will be more on the dilution side. Therefore, more controlled studies involving both microstructure and loading variations shall be explored. Furthermore, the effects of crystallographic texture and spatial grain orientation on HE remain significantly under-explored in the literature. Consequently, systematic studies are required to decouple these competing mechanisms in AM materials.

3. Nano-scale

HE mechanisms can be further elucidated from a nanoscale perspective. Hydrogen is believed to occupy atomic vacancies or replace matrix atoms, weakening interatomic bonding and mechanical properties [205]. However, those assumptions await verification through in-situ nanoscale hydrogen movement recording, hindered by the volatility of hydrogen atoms. This stagnation hindered the mitigation of HE from molecular dynamics.

7.4. Alloying systems

Screening all the reviewed AM alloys, it is evident that Fe-based stainless steels have been investigated more extensively than other alloy systems. In Fe-based systems, the γ-austenite matrix with an FCC structure generally exhibits higher resistance to HE than BCC phases, as the significantly higher hydrogen diffusivity in BCC structures promotes hydrogen accumulation and facilitates HE-induced cracking [206]. Consequently, research efforts have predominantly focused on γ-austenitic stainless steels.

A significant gap remains between the mature and rich data of Fe-based alloys and the limited data on Ni-based, Ti-based, and Cu-based systems. These materials are essential for severe environments, such as cryogenic liquid hydrogen storage, yet their behavior in AM forms is not fully understood and explored. Overall, future research should move beyond simply testing standard commercial powders. Instead, the focus must shift to "Alloy design for AM" specifically for hydrogen applications. This means adjusting the chemical composition of powders to prevent the formation of harmful phases (like the brittle δ phase in Ni-alloys) during the printing process itself, rather than relying solely on post-process heat treatments. Furthermore, the emerging alloys, such as HEAs, with the capability for MMAM, present a new opportunity to decouple mechanical strength from hydrogen susceptibility, as demonstrated in section 7.2. By strategically grading material composition, for instance, printing a hydrogen-impermeable high-entropy skin over a ductile, high-toughness or high-strength metallic core, AM offers the unique potential to engineer component-level resistance with new alloys that monolithic materials cannot achieve.

8. Conclusions and outlook

In this article, we have undertaken a comprehensive review of the current state of knowledge about the phenomenon of hydrogen embrittlement (HE) in metallic materials fabricated through additive manufacturing (AM) to support the transition from fossil fuels to hydrogen energy. This transition has the potential to reduce greenhouse gas emissions and enhance the sustainability of structural components operating in different hydrogen environments. Noteworthy conclusions and outlooks can be drawn.

(1) On the component level, compared with the traditional fabrication method, AM offers a distinct advantage in its capacity for high manufacturing flexibility concerning shape, microstructure design, and the integration of in-situ processing. These advantages hold the potential to mitigate the effects of HE in AM-fabricated components to avoid the additional processes of joining, welding, cutting, etc. in the conventional manufacturing processes, which are more prone to hydrogen embrittlement. In addition, these benefits help minimize material usage, which in turn promotes the sustainability of components.

(2) The prospects for the application of AM to alleviate HE-related issues in the industry are promising. However, this potential is constrained by several key challenges, including comparatively low efficiency, elevated fabrication costs, and a relatively high porosity rate in as-fabricated samples. High residual stresses also compromise the HE resistance of as-fabricated AM samples. In the aerospace sector, there is a discernible shift towards AM as a replacement for conventional manufacturing methods, particularly for producing components intended for service in HE-prone environments. Notably, mass production of certain parts such as nozzles has already been achieved. Regrettably, in other application domains, the adoption of AM remains largely confined to laboratory settings or small-batch production.

(3) On the material level, the direct comparison of the HE susceptibility between AM-fabricated and conventional materials shows controversial results, which are related to inconsistent effects of certain microstructure features on the HE mechanisms. The influence of grain size and dislocation density on the HE resistance of AM-fabricated components is a subject of interest. However, the precise conditions that trigger either positive or negative effects remain unclear. Defects, secondary phases, and the presence of molten pools are generally associated with diminished HE resistance in most instances. These microstructures can be influenced by various factors, including processing parameters, processing methods, and additional physical or thermal treatments. Nevertheless, the underlying mechanisms responsible for these effects in AM-fabricated components remain incompletely understood. Consequently, more comprehensive and systematic investigations are warranted to elucidate the influence of microstructure and processing parameters on HE resistance in AM-fabricated materials. Given the intricacies of the HE mechanism, there is an urgent need to develop novel methods to mitigate HE corrosion. In the author's view, LSP, remelting, and controlling the pausing time during manufacturing should be areas of focus for future research.

(4) On the practical level, the current research on the HE susceptibility of AM-fabricated materials is mainly using the electrochemical charging method, which makes sense for many industry sectors involving aqueous conditions, such as seawater,

rainwater, acidic solutions, etc. However, for future applications related to using hydrogen as an energy supplier, the gaseous and liquid hydrogen environments are more relevant to evaluate the HE susceptibility. Therefore, future studies using gaseous and liquid hydrogen charing are strongly encouraged for the wide application of AM-fabricated metallic materials in the hydrogen processing, transportation, and storage sectors. In addition to the charging methods, more versatile testing methods for HE (e.g., Charpy, fracture toughness, fatigue tests) and quantification methods of hydrogen diffusion are also needed in future studies, as the current literature mainly focuses on tensile properties for the HE analysis and thermal desorption spectroscopy for the hydrogen update behavior.

(5) Despite the inherent limitations of AM, there are two particularly promising avenues for its application. First, the production of large-scale components via AM holds significant potential. Second, there is growing interest in employing AM in the energy industry to fabricate components intended for service in HE-prone environments. Third, there is still substantial room for researchers to investigate the fundamental mechanisms and to build a more complete picture of how hydrogen interacts with different AM-fabricated alloy systems. Both of these areas present exciting opportunities for the future development of AM technologies.

(6) Given the inherent complexity and multi-scale nature of HE phenomena in AM metallic materials with microstructural features such as melt pool boundaries, anisotropic grain structures, and complex residual stress patterns, etc., there is a clear need for advanced modeling and simulation methods tailored specifically for HE in AM metals. Future research shall prioritize developing predictive multi-scale models, integrating models across scales, e.g., molecular dynamics, phase-field modeling, crystal plasticity methods, and finally continuum models with hydrogen transport simulations. Such computational approaches are essential to systematically understand, predict, and quantify HE behavior in AM metallic components, ultimately guiding materials design to mitigate HE.

Declaration of generative AI in scientific writing

During the preparation of this work, the authors used ChatGPT to improve the readability and language. After using this tool, the authors reviewed and edited the content as needed and took full responsibility for the content of the publication.

CRediT authorship contribution statement

Shengzhao Yang: Conceptualization, Methodology, Writing – original draft. **Rongfei Juan:** Visualization, Writing – review & editing. **Junhe Lian:** Conceptualization, Funding acquisition, Methodology, Supervision, Validation, Writing – review & editing.

Declaration of competing interest

The authors declare that they have no known competing financial interests or personal relationships that could have appeared to influence the work reported in this paper.

Acknowledgments

The funding from the Technology Industries of Finland Centennial Foundation and Jane and Aatos Erkko Foundation via the Future Makers Lian Funding Program is acknowledged (project No. 2617). Co-funded by the European Union (ERC, HIGMAM, 101078829). Views and opinions expressed are however those of the authors only and do not necessarily reflect those of the European Union. European Union cannot be held responsible for them.

Data availability

No data was used for the research described in the article.

References

[1] H. Ritchie, M. Roser, CO_2 emissions. https://ourworldindata.org/co2-emissions, 2024. (Accessed 20 October 2025).
[2] M.W. Jones, G.P. Peters, T. Gasser, R.M. Andrew, C. Schwingshackl, J. Gutschow, R.A. Houghton, P. Friedlingstein, J. Pongratz, C. Le Quere, National contributions to climate change due to historical emissions of carbon dioxide, methane, and nitrous oxide since 1850, Sci. Data 10 (1) (2023) 155, https://doi.org/10.1038/s41597-023-02041-1.
[3] A.E. Matveev, Energy-efficient scientific-technological approaches to the processing of plastic waste PET, PE, PP, PS to produce hydrogen-containing gas and titanium carbide powder, Mater. Today Sustain. 27 (2024), https://doi.org/10.1016/j.mtsust.2024.100802.
[4] Y. Shi, S. Zhang, X. Liu, S. Wang, B. Gao, J. Wang, Recent advances in hydrogen spillover and reverse hydrogen spillover for the two-dimensional materials, Mater. Today Sustain. 31 (2025), https://doi.org/10.1016/j.mtsust.2025.101194.
[5] Y.C. Tak, J.K.S. Paw, K. Kadirgama, T. Yusaf, D. Ramasamy, K. Sudhakar, M. Sandhya, O.I. Awad, B. Zhou, J. Pasupuleti, L. Samylingam, R.K. Rajamony, Decarbonizing the future for the transportation and aviation industries: green hydrogen as the sustainable fuel solution, Mater. Today Sustain. 31 (2025), https://doi.org/10.1016/j.mtsust.2025.101152.
[6] G. Corchero, J.L. Montañés, An approach to the use of hydrogen for commercial aircraft engines, J. Aero. Eng. 219 (1) (2005) 35–44, https://doi.org/10.1243/095441005X9139.
[7] T. Yusaf, L. Fernandes, A.R.A. Talib, Y.S.M. Altarazi, W. Alrefae, K. Kadirgama, D. Ramasamy, A. Jayasuriya, G. Brown, R. Mamat, H.A. Dhahad, F. Benedict, M. Laimon, Sustainable aviation—hydrogen is the future, Sustainability 14 (2022) 548, https://doi.org/10.3390/su14010548.
[8] Publications Office of the European Union, Hydrogen Roadmap Europe: a Sustainable Pathway for the European Energy Transition, 2016. https://op.europa.eu/en/publication-detail/-/publication/0817d60d-332f-11e9-8d04-01aa75ed71a1/language-en. (Accessed 20 October 2025).
[9] Shibani, M. Davis, S. Radpour, A. Kumar, Assessment of low-carbon hydrogen integration into natural gas energy systems beyond blending: an analysis of pure H2 communities in a natural gas-dependent region, J. Clean. Prod. 518 (2025) 145869, https://doi.org/10.1016/j.jclepro.2025.145869.
[10] M. Liu, L. Jiang, M.J. Demkowicz, Role of slip in hydrogen-assisted crack initiation in Ni-based alloy 725, Sci. Adv. 10 (29) (2024) e2118, https://doi.org/10.1126/sciadv.ado2118.
[11] Z.A. Luo, L.Y. Mao, C. Huang, H.Y. Zhou, M.K. Wang, A strategy for simultaneously enhancing mechanical strength and hydrogen embrittlement resistance: exceptional performance of laminated metal composite in hydrogen environments, Mater. Des. 237 (2024) 112549, https://doi.org/10.1016/j.matdes.2023.112549.
[12] H. Ma, L. Sun, H. Luo, X. Li, Hydrogen embrittlement of high-strength marine steel as a weld joint in artificial seawater under cathodic polarization, Eng. Fail. Anal. 134 (2022) 106044, https://doi.org/10.1016/j.engfailanal.2022.106044.
[13] A.M. Lancha, M. Serrano, J. Lapenã, D. Goà Mez-Bricenã, Failure analysis of a river water circulating pump shaft from a NPP, Eng. Fail. Anal. 8 (3) (2001) 271–291, https://doi.org/10.1016/S1350-6307(00)00005-4.
[14] Y. Aboura, A.J. Garner, R. Euesden, Z. Barrett, C. Engel, N.J.H. Holroyd, P. B. Prangnell, T.L. Burnett, Understanding the environmentally assisted cracking (EAC) initiation and propagation of new generation 7xxx alloys using slow strain rate testing, Corros. Sci. 199 (2022) 110161, https://doi.org/10.1016/j.corsci.2022.110161.
[15] M. Chen, S. Liu, K. He, X. Zheng, Y. Zhang, J. Tang, L. Ye, Hydrogen-induced failure in a partially-recrystallized al-zn-mg-cu alloy with different aging conditions: influence of deformation behavior dominated by microstructures, Mater. Des. 233 (2023) 112199, https://doi.org/10.1016/j.matdes.2023.112199.
[16] M. Iannuzzi, G.S. Frankel, The carbon footprint of steel corrosion, npj Mater. Degrad. 6 (1) (2022) 101, https://doi.org/10.1038/s41529-022-00318-1.
[17] O. Güvenç, R. Lizarde, C.C. Tasan, Solid-state steelmaking by scrap consolidation: a processing pathway with minimal energy and CO2 burdens, J. Clean. Prod. 452 (2024), https://doi.org/10.1016/j.jclepro.2024.141976.
[18] J. Wang, L.J. Ma, M. Han, J. Jia, H.S. Wu, X. Zhang, Molecular and dissociated adsorption of hydrogen on TiC6H6, Int. J. Hydrogen Energy 44 (47) (2019) 25800–25808, https://doi.org/10.1016/j.ijhydene.2019.08.016.
[19] P. Metalnikov, D. Eliezer, G. Ben-Hamu, E. Tal-Gutelmacher, Y. Gelbstein, C. Munteanu, Hydrogen embrittlement of electron beam melted Ti–6Al–4V, J. Mater. Res. Technol. 9 (6) (2020) 16126–16134, https://doi.org/10.1016/j.jmrt.2020.11.073.
[20] P. Gong, J. Nutter, P.E.J. Rivera-Diaz-Del-Castillo, W.M. Rainforth, Hydrogen embrittlement through the formation of low-energy dislocation nanostructures in nanoprecipitation-strengthened steels, Sci. Adv. 6 (46) (2020), https://doi.org/10.1126/sciadv.abb6152.

[21] D. Wu, L. Cui, X. Wu, X. Guo, W. Shao, Z. Tan, D. He, Cold metal transfer welding of AlSi7Mg alloy sheets prepared by selective laser melting, J. Manuf. Process. 84 (2022) 282–297, https://doi.org/10.1016/j.jmapro.2022.10.013.
[22] Z. Zhang, Z. Guo, Q. Han, D. Hu, S. Wu, H. Fan, E. Li, M. Li, Y. Xu, S. Yang, C. Huang, W. Yan, Anomalous anisotropy in an additively manufactured solid-solution-strengthened superalloy from room to elevated temperatures, Int. J. Plast. 192 (2025), https://doi.org/10.1016/j.ijplas.2025.104409.
[23] Q. Sun, G. Zhi, S. Zhou, R. Tao, J. Qi, Compressive mechanical and heat conduction properties of AlSi10Mg gradient metamaterials fabricated via laser powder bed fusion, Chin. J. Mech. Eng. 37 (1) (2024) 1–18, https://doi.org/10.1186/s10033-024-01122-5.
[24] Z. Zhang, Q. Han, Z. Liu, J. Gao, L. Wang, H. Liu, R. Wang, T. Ma, Z. Gao, Combined effects of heat treatment and TiB2 content on the high-temperature tensile performance of TiB2-modified Ni-based GH3230 alloy processed by laser powder bed fusion, Mater. Sci. Eng. A 861 (2022) 144379, https://doi.org/10.1016/j.msea.2022.144379.
[25] Y. Yin, J. Zhang, J. Gao, Z. Zhang, Q. Han, Z. Zan, Laser powder bed fusion of Ni-based hastelloy X superalloy: microstructure, anisotropic mechanical properties and strengthening mechanisms, Mater. Sci. Eng., A 827 (2021) 142076, https://doi.org/10.1016/j.msea.2021.142076, 142076.
[26] Z. Zhang, Q. Han, S. Yang, Y. Yin, J. Gao, R. Setchi, Laser powder bed fusion of advanced submicrometer TiB2 reinforced high-performance Ni-based composite, Mater. Sci. Eng. A 817 (2021) 141416, https://doi.org/10.1016/j.msea.2021.141416, 141416.
[27] Q. Sun, D. Geng, J. Guo, S. Zhou, M. Chen, R. Tao, Numerical and experimental analysis of hydraulic and thermal performance in additively manufactured topology-optimized heat sinks with different geometric features, Appl. Therm. Eng. (2025) 126619, https://doi.org/10.1016/j.applthermaleng.2025.126619.
[28] S. Singh, R.P. Mohanty, S.K. Mangla, V. Agrawal, Critical success factors of additive manufacturing for higher sustainable competitive advantage in supply chains, J. Clean. Prod. 425 (2023) 138908, https://doi.org/10.1016/j.jclepro.2023.138908.
[29] F. Sanguineti, G. Magnani, A. Zucchella, Technology adoption, global value chains and sustainability: the case of additive manufacturing, J. Clean. Prod. 408 (2023), https://doi.org/10.1016/j.jclepro.2023.137095.
[30] N. Top, I. Sahin, S.K. Mangla, M.D. Sezer, Y. Kazancoglu, Towards sustainable production for transition to additive manufacturing: a case study in the manufacturing industry, Int. J. Prod. Res. 61 (13) (2022) 4450–4471, https://doi.org/10.1080/00207543.2022.2152895.
[31] C. Han, Q. Fang, Y. Shi, S.B. Tor, C.K. Chua, K. Zhou, Recent advances on high-entropy alloys for 3D printing, Adv. Mater. 32 (26) (2020) e1903855, https://doi.org/10.1002/adma.201903855.
[32] N.A. Aziz, N.A.A. Adnan, D.A. Wahab, A.H. Azman, Component design optimisation based on artificial intelligence in support of additive manufacturing repair and restoration: current status and future outlook for remanufacturing, J. Clean. Prod. 296 (2021), https://doi.org/10.1016/j.jclepro.2021.126401.
[33] M. Christ, X. Guo, R. Sharma, T. Li, W. Bleck, U. Reisgen, Hydrogen embrittlement susceptibility of gas metal arc welded joints from a high-strength low-alloy steel grade S690QL, Steel Res. Int. 91 (11) (2020) 200013, https://doi.org/10.1002/srin.202000131.
[34] N. Nanninga, J. Grochowsi, L. Heldt, K. Rundman, Role of microstructure, composition and hardness in resisting hydrogen embrittlement of fastener grade steels, Corros. Sci. 52 (4) (2010) 1237–1246, https://doi.org/10.1016/j.corsci.2009.12.020.
[35] D. Hardie, S.e. Liu, The effect of stress concentration on hydrogen embrittlement of a low alloy steel, Corros. Sci. 38 (5) (1996) 721–733, https://doi.org/10.1016/0010-938X(96)00161-8.
[36] Z. Sheng, C. Altenbach, U. Prahl, D. Zander, W. Bleck, Effect of cutting method on hydrogen embrittlement of high-Mn TWIP steel, Mater. Sci. Eng. A 744 (2019) 10–20, https://doi.org/10.1016/j.msea.2018.11.128.
[37] T.S. Singhal, J.K. Jain, M. Kumar, V. Bhojak, K.K. Saxena, D. Buddhi, C. Prakash, A comprehensive comparative review: welding and additive manufacturing, Int. J. Interact. Des. Manuf. 18 (3) (2023) 1829–1843, https://doi.org/10.1007/s12008-022-01152-0.
[38] N. Xu, N. Ding, J. Shi, W. Guo, C.M.L. Wu, Fracture failure of zinc-plated hub bolts by hydrogen embrittlement, J. Fail. Anal. Prev. 15 (4) (2015) 464–469, https://doi.org/10.1007/s11668-015-9972-1.
[39] S.D. Wu, W.Y. Cheng, J.H.C. Yang, C.H. Yang, S.Y. Liao, The corrosion protection study on inner surface from welding of aluminum alloy 7075-T6 hydrogen storage bottle, Int. J. Hydrogen Energy 41 (1) (2016) 570–596, https://doi.org/10.1016/j.ijhydene.2015.09.144.
[40] R.O. Cunha Lima, C. Alves, A.C.A.d. Melo, S.M. Alves, L. Araújo Filho, New technique for deposition and thermochemical treatment of small parts with complex geometry applied to machining inserts, J. Mater. Res. Technol. 9 (6) (2020) 15811–15823, https://doi.org/10.1016/j.jmrt.2020.11.047.
[41] T. Gualtieri, A. Bandyopadhyay, Additive manufacturing of compositionally gradient metal-ceramic structures: stainless steel to vanadium carbide, Mater. Des. 139 (2018) 419–428, https://doi.org/10.1016/j.matdes.2017.11.007.
[42] S. Yang, Q. Han, Y. Yin, Z. Zhang, L. Wang, Z. Zhu, H. Liu, T. Ma, Z. Gao, Effects of TiB2 content on the processability and mechanical performance of Hastelloy-X based composites fabricated by selective laser melting, Opt. Laser Technol. 155 (2022) 108441, https://doi.org/10.1016/j.optlastec.2022.108441.
[43] S.-W. Baek, E.J. Song, J.H. Kim, M. Jung, U.B. Baek, S.H. Nahm, Hydrogen embrittlement of 3-D printing manufactured austenitic stainless steel part for hydrogen service, Scripta Mater. 130 (2017) 87–90, https://doi.org/10.1016/j.scriptamat.2016.11.020.
[44] D. Wan, S. Guan, D. Wang, X. Lu, J. Ma, Hydrogen embrittlement of additively manufactured AlCoCrFeNi2.1 eutectic high-entropy alloy, Corros. Sci. 195 (2022) 110007, https://doi.org/10.1016/j.corsci.2021.110007.
[45] S. Ghods, E. Schultz, C. Wisdom, R. Schur, R. Pahuja, A. Montelione, D. Arola, M. Ramulu, Electron beam additive manufacturing of Ti6Al4V: evolution of powder morphology and part microstructure with powder reuse, Materialia 9 (2020) 100631, https://doi.org/10.1016/j.mtla.2020.100631.
[46] S. Gruber, C. Grunert, M. Riede, E. López, A. Marquardt, F. Brueckner, C. Leyens, Comparison of dimensional accuracy and tolerances of powder bed based and nozzle based additive manufacturing processes, J. Laser Appl. 32 (3) (2020) 32016, https://doi.org/10.2351/7.0000115, 032016.
[47] C. Sun, Y. Wang, M.D. McMurtrey, N.D. Jerred, F. Liou, J. Li, Additive manufacturing for energy: a review, Appl. Energy 282 (2021) 116041, https://doi.org/10.1016/j.apenergy.2020.116041.
[48] B. DeBoer, N. Nguyen, F. Diba, A. Hosseini, Additive, subtractive, and formative manufacturing of metal components: a life cycle assessment comparison, J. Adv. Manuf. Technol. 115 (1) (2021) 413–432, https://doi.org/10.1007/s00170-021-07173-5.
[49] S. Kumar, Development of functionally graded materials by ultrasonic consolidation, CIRP J. Manuf. Sci. Technol. 3 (1) (2010) 85–87, https://doi.org/10.1016/j.cirpj.2010.07.006.
[50] J.W. Lee, I.H. Lee, D.W. Cho, Development of micro-stereolithography technology using metal powder, Microelectron. Eng. 83 (4-9) (2006) 1253–1256, https://doi.org/10.1016/j.mee.2006.01.192. SPEC. ISS.
[51] P.J. Bartolo, J. Gaspar, Metal filled resin for stereolithography metal part, CIRP Ann. Manuf. Technol. 57 (1) (2008) 235–238, https://doi.org/10.1016/j.cirp.2008.03.124.
[52] K. Rajan, M. Samykano, K. Kadirgama, W.S.W. Harun, M.M. Rahman, Fused deposition modeling: process, materials, parameters, properties, and applications, Int. J. Adv. Manuf. Technol. 120 (2022) 1531–1570, https://doi.org/10.1007/s00170-022-08860-7.
[53] Y. Bai, C.B. Williams, Binder jetting additive manufacturing with a particle-free metal ink as a binder precursor, Mater. Des. 147 (2018) 146–156, https://doi.org/10.1016/j.matdes.2018.03.027.
[54] T.D. Grant, A.C. Hourd, S. Zolotovskaya, J.B. Lowe, R.J. Rothwell, T.D.A. Jones, A. Abdolvand, Inkjet printing of high-concentration particle-free platinum inks, Mater. Des. 214 (2022) 110377, https://doi.org/10.1016/j.matdes.2021.110377.
[55] GE additive, New manufacturing milestone: 30,000 additive fuel nozzles. https://www.ge.com/additive/stories/new-manufacturing-milestone-30000-additive-fuel-nozzles, 2018. (Accessed 20 October 2025).
[56] P.R. Gradl, C.S. Protz, D.L. Ellis, S.E. Greene, Progress in Additively Manufactured Copper-Alloy GRCop-84, GRCop-42, and Bimetallic Combustion Chambers for Liquid Rocket Engines, 70th International Astronautical Congress, U.S. Government, 2019, pp. 21–25.
[57] D. Cecere, E. Giacomazzi, A. Ingenito, A review on hydrogen industrial aerospace applications, Int. J. Hydrogen Energy 39 (2014) 10731–10747, https://doi.org/10.1016/j.ijhydene.2014.04.126.
[58] Y. Qiu, H. Yang, L. Tong, L. Wang, Research progress of cryogenic materials for storage and transportation of liquid hydrogen, Metals 11 (2021) 1101, https://doi.org/10.3390/met11071101.
[59] T. Pan, X. Zhang, T. Yamazaki, A. Sutton, W. Cui, L. Li, F. Liou, Characteristics of inconel 625—copper bimetallic structure fabricated by directed energy deposition, Int. J. Adv. Manuf. Technol. 109 (5-6) (2020) 1261–1274, https://doi.org/10.1007/s00170-020-05713-z.
[60] Q. Han, R. Mertens, M.L. Montero-Sistiaga, S. Yang, R. Setchi, K. Vanmeensel, B. Van Hooreweder, S.L. Evans, H. Fan, Laser powder bed fusion of hastelloy X: effects of hot isostatic pressing and the hot cracking mechanism, Mater. Sci. Eng. A 732 (2018) 228–239, https://doi.org/10.1016/j.msea.2018.07.008.
[61] R.P. Gangloff, B.P. Somerday, Gaseous Hydrogen Embrittlement of Materials in Energy Technologies: the Problem, its Characterisation and Effects on Particular Alloy Classes, Elsevier, 2012.
[62] B. Blakey-Milner, P. Gradl, G. Snedden, M. Brooks, J. Pitot, E. Lopez, M. Leary, F. Berto, A. du Plessis, Metal additive manufacturing in aerospace: a review, Mater. Des. 209 (2021) 110008, https://doi.org/10.1016/j.matdes.2021.110008.
[63] S.S.I. cooperation, Managing ship life cycle – prepare for ship's lifespan. https://www.ssi-corporate.com/content/managing-ship-life-cycle-prepare-for-ships-lifespan/. (Accessed 20 October 2025).
[64] P. Michael, The lifespan of planes: how long can they stay in service?. https://executiveflyers.com/how-long-do-planes-last/, 2023. (Accessed 20 October 2025).
[65] T. Matsuda, S. Hanaoka, T. Kawasaki, Cost analysis of bulk cargo containerization, Maritime Pol. Manage. 47 (6) (2020) 736–755, https://doi.org/10.1080/03088839.2020.1727036.
[66] R. Simon, 3D-printed spare parts revolutionize maritime supply chain. https://www.dnv.com/expert-story/maritime-impact/3D-printed-spare-parts-revolutionize-maritime-supply-chain/, 2020. (Accessed 20 October 2025).
[67] M. Ziółkowski, T. Dyl, Possible applications of additive manufacturing technologies in shipbuilding: a review, Machines 8 (4) (2020) 1–34, https://doi.org/10.3390/machines8040084.
[68] F. Jake, RAMLAB gets closer to world's first 3D printed props. https://www.ramlab.com/resources/ramlab-unveils-worlds-first-class-approved-3d-printed-ships-propeller/, 2017. (Accessed 20 October 2025).
[69] J. Eva, G. Ramesh Babu, Additive manufacturing enters the maritime mainstream. https://www.dnv.com/expert-story/maritime-impact/Additive-Manufacturing-enters-the-maritime-mainstream/, 2022. (Accessed 20 October 2025).

[70] R. Tali, 3D printing metal parts on a ship-what does the navy require to make the dream a reality?. https://www.navy.mil/Press-Office/News-Stories/Article/3209860/metal-3d-printer-installed-on-uss-bataan/, 2022. (Accessed 20 October 2025).
[71] İ. Baylakoğlu, A. Fortier, S. Kyeong, R. Ambat, H. Conseil-Gudla, M.H. Azarian, M.G. Pecht, The detrimental effects of water on electronic devices, e-Prime - advances in electrical Engineering, Electronics and Energy 1 (2021) 100016, https://doi.org/10.1016/j.prime.2021.100016.
[72] S. Kumar, R.S. Bharj, Emerging composite material use in current electric vehicle: a review, Mater. Today proc. 5 (2018) 27946–27954, https://doi.org/10.1016/j.matpr.2018.10.034.
[73] T.S. Tshephe, S.O. Akinwamide, E. Olevsky, P.A. Olubambi, Additive manufacturing of titanium-based alloys- A review of methods, properties, challenges, and prospects, Heliyon 8 (2022) e09041, https://doi.org/10.1016/j.heliyon.2022.e09041.
[74] M. Kremenetsky, BMW begins production of hydrogen-powered iX5 vehicle with 3D printed parts. https://3dprint.com/296197/bmw-begins-production-of-hydrogen-powered-ix5-vehicle-with-3d-printed-parts/, 2022. (Accessed 20 October 2025).
[75] F. Sartipi, A. Sartipi, Brief review on advancements in construction additive manufacturing, J. Constr. Mater. 1 (2) (2020) 1–11, https://doi.org/10.36756/JCM.v1.2.4.
[76] B.O. Omiyale, T.O. Olugbade, T.E. Abioye, P.K. Farayibi, Wire arc additive manufacturing of aluminium alloys for aerospace and automotive applications: a review, Mater. Sci. Technol. 38 (2022) 391–408, https://doi.org/10.1080/02670836.2022.2045549.
[77] A.R. Kannan, S.M. Kumar, R. Pramod, N.S. Shanmugam, M. Vishnukumar, S. Naveenkumar, Microstructural characterization and mechanical integrity of stainless steel 316L clad layers deposited via wire arc additive manufacturing for nuclear applications, Mater. Werkst. 52 (6) (2021) 617–623, https://doi.org/10.1002/mawe.202000242.
[78] Q. Cheng, N. Guo, Y. Fu, D. Zhang, G. Wang, M. Yu, Underwater wire-feed laser deposition of thin - walled tubular structure of aluminum alloy, J. Manuf. Process. 67 (2021) 56–62, https://doi.org/10.1016/j.jmapro.2021.04.032.
[79] Z.D. Wang, G.F. Sun, M.Z. Chen, Y. Lu, S.B. Zhang, H.F. Lan, K.D. Bi, Z.H. Ni, Investigation of the underwater laser directed energy deposition technique for the on-site repair of HSLA-100 steel with excellent performance, Addit. Manuf. 39 (2021) 101884, https://doi.org/10.1016/j.addma.2021.101884.
[80] N. Guo, X. Zhang, Y. Fu, W. Luo, H. Chen, J. Long He, A novel strategy to prevent hydrogen charging via spontaneously molten-slag-covering droplet transfer mode in underwater wet FCAW, Mater. Des. 226 (2023) 111636, https://doi.org/10.1016/j.matdes.2023.111636.
[81] S.K. Dwivedi, M. Vishwakarma, Hydrogen embrittlement in different materials: a review, Int. J. Hydrogen Energy 43 (2018) 21603–21616, https://doi.org/10.1016/j.ijhydene.2018.09.201.
[82] L. Huang, D. Chen, D. Xie, S. Li, Y. Zhang, T. Zhu, D. Raabe, E. Ma, J. Li, Z. Shan, Quantitative tests revealing hydrogen-enhanced dislocation motion in alpha-iron, Nat. Mater. 22 (6) (2023) 710–716, https://doi.org/10.1038/s41563-023-01537-w.
[83] Y.-S. Chen, C. Huang, P.-Y. Liu, H.-W. Yen, R. Niu, P. Burr, K.L. Moore, E. Martínez-Pañeda, A. Atrens, J.M. Cairney, Hydrogen trapping and embrittlement in metals – a review, Int. J. Hydrogen Energy (2024) 789–821, https://doi.org/10.1016/j.ijhydene.2024.04.076.
[84] D. Xie, S. Li, M. Li, Z. Wang, P. Gumbsch, J. Sun, E. Ma, J. Li, Z. Shan, Hydrogenated vacancies lock dislocations in aluminium, Nat Com 7 (2016) 13341, https://doi.org/10.1038/ncomms13341.
[85] J. Song, W.A. Curtin, Mechanisms of hydrogen-enhanced localized plasticity: an atomistic study using α-Fe as a model system, Acta Mater. 68 (2014) 61–69, https://doi.org/10.1016/j.actamat.2014.01.008.
[86] X. Li, X. Ma, J. Zhang, E. Akiyama, Y. Wang, X. Song, Review of hydrogen embrittlement in metals: hydrogen diffusion, hydrogen characterization, hydrogen embrittlement mechanism and prevention, ACTA METALL. SIN. 33 (2020) 759–773, https://doi.org/10.1007/s40195-020-01039-7.
[87] P.L. Bessemer, The effect of occluded hydrogen on the tensile strength of iron, Proc. Roy. Soc. Lond. A 112 (1926) 182–195, https://doi.org/10.1098/rspa.1926.0103.
[88] M.B. Djukic, G.M. Bakic, V. Sijacki Zeravcic, A. Sedmak, B. Rajicic, The synergistic action and interplay of hydrogen embrittlement mechanisms in steels and iron: localized plasticity and decohesion, Eng. Fract. Mech. 216 (2019) 106528, https://doi.org/10.1016/j.engfracmech.2019.106528.
[89] B. Tekkaya, J. Wu, M. Dölz, J. Lian, S. Münstermann, Coupled chemical–mechanical damage modeling of hydrogen-induced material degradation, Eng. Fract. Mech. 314 (2025), https://doi.org/10.1016/j.engfracmech.2024.110751.
[90] S. Hu, Y. Yin, H. Liang, Y. Zhang, Y. Yan, A quantification study of hydrogen-induced cohesion reduction at the atomic scale, Mater. Des. 218 (2022) 110702, https://doi.org/10.1016/j.matdes.2022.110702.
[91] X. Li, J. Zhang, Q. Fu, X. Song, S. Shen, Q. Li, A comparative study of hydrogen embrittlement of 20SiMn2CrNiMo, PSB1080 and PH13-8Mo high strength steels, Mater. Sci. Eng., A 724 (2018) 518–528, https://doi.org/10.1016/j.msea.2018.03.076.
[92] S.P. Lynch, Hydrogen embrittlement (HE) phenomena and mechanisms, Stress Corrosion Cracking (2011) 90–130.
[93] M. Nagumo, Hydrogen related failure of steels - a new aspect, Mater. Sci. Technol. (2004) 940–950, https://doi.org/10.1179/026708304225019687.
[94] M. Nagumo, K. Takai, The predominant role of strain-induced vacancies in hydrogen embrittlement of steels: overview, Acta Mater. 165 (2019) 722–733, https://doi.org/10.1016/j.actamat.2018.12.013.
[95] M.D. Dolan, M.A. Kochanek, C.N. Munnings, K.G. McLennan, D.M. Viano, Hydride phase equilibria in V-Ti-Ni alloy membranes, J. Alloys Compd. 622 (2015) 276–281, https://doi.org/10.1016/j.jallcom.2014.10.081.
[96] L. Vergani, C. Colombo, G. Gobbi, F.M. Bolzoni, G. Fumagalli, Hydrogen effect on fatigue behavior of a quenched&tempered steel, Procedia Eng. 74 (2014) 468–471, https://doi.org/10.1016/j.proeng.2014.06.299.
[97] S. Rahimi, K. Verbeken, T. Depover, E. Proverbio, Hydrogen embrittlement of pipeline steels under gaseous and electrochemical charging: a comparative review on tensile properties, Eng. Fail. Anal. 167 (2025), https://doi.org/10.1016/j.engfailanal.2024.108956.
[98] P. Rozenak, Effects of nitrogen on hydrogen embrittlement in AISI type 316, 321 and 347 austenitic stainless steels, J. Mater. Sci. 25 (1990) 2532–2538, https://doi.org/10.1115/PVP2010-25698.
[99] D. Eliezer, The behaviour of 316l stainless steel in hydrogen, J. Mater. Sci. 19 (1984) 1540–1547, https://doi.org/10.1007/BF00563051.
[100] Y. Liu, Y. Chen, C. Yang, J. Lian, Y. Feng, X. Han, The effect of charging conditions on hydrogen embrittlement behavior of ultra-high-strength steel 22MnB5, Mater. Charact. 194 (2022) 112377, https://doi.org/10.1016/j.matchar.2022.112377.
[101] F. Dong, J. Venezuela, H. Li, Z. Shi, Q. Zhou, L. Chen, J. Chen, L. Du, A. Atrens, Effect of vanadium and rare earth microalloying on the hydrogen embrittlement susceptibility of a Fe-18Mn-0.6C TWIP steel studied using the linearly increasing stress test, Corros. Sci. 185 (2021) 109440, https://doi.org/10.1016/j.corsci.2021.109440.
[102] A. Barnoush, H. Vehoff, Electrochemical nanoindentation: a new approach to probe hydrogen/deformation interaction, Scripta Mater. 55 (2) (2006) 195–198, https://doi.org/10.1016/j.scriptamat.2006.03.041.
[103] T. Hajilou, M.S.B. Hope, A.H. Zavieh, N. Kheradmand, R. Johnsen, A. Barnoush, In situ small-scale hydrogen embrittlement testing made easy: an electrolyte for preserving surface integrity at nano-scale during hydrogen charging, Int. J. Hydrogen Energy 43 (27) (2018) 12516–12529, https://doi.org/10.1016/j.ijhydene.2018.04.168.
[104] A. Pradhan, M. Vishwakarma, S.K. Dwivedi, A review: the impact of hydrogen embrittlement on the fatigue strength of high strength steel, Mater. Today proc. 26 (2019) 3015–3019, https://doi.org/10.1016/j.matpr.2020.02.627.
[105] M. Cauwels, R. Depraetere, W. De Waele, S. Hertelé, K. Verbeken, T. Depover, Effect of hydrogen charging on charpy impact toughness of an X70 pipeline steel, Procedia Struct. Integr. 42 (2022) 977–984, https://doi.org/10.1016/j.prostr.2022.12.123.
[106] E. Fangnon, E. Malitckii, Y. Yagodzinskyy, P. Vilaca, Improved accuracy of thermal desorption spectroscopy by specimen cooling during measurement of hydrogen concentration in a high-strength steel, Materials 13 (5) (2020) 1252, https://doi.org/10.3390/ma13051252.
[107] M. Safyari, M. Moshtaghi, T. Hojo, E. Akiyama, Mechanisms of hydrogen embrittlement in high-strength aluminum alloys containing coherent or incoherent dispersoids, Corros. Sci. 194 (2022) 109895, https://doi.org/10.1016/j.corsci.2021.109895.
[108] X. Lu, D. Wang, R. Johnsen, Hydrogen diffusion and trapping in nickel-based alloy 625: an electrochemical permeation study, Electrochim. Acta 421 (2022), https://doi.org/10.1016/j.electacta.2022.140477.
[109] W.Y. Choo, J.Y. Lee, Thermal analysis of trapped hydrogen in pure iron, Metall. Mater. Trans. A 13 (1982) 135–140, https://doi.org/10.1007/BF02642424.
[110] R. Liu, D. Liu, J. Li, S. Liu, Z. Liu, L. Gao, X. Jia, S. Ao, Improved understanding of the sulfidization mechanism in cerussite flotation: an XPS, ToF-SIMS and FESEM investigation, Colloids Surf. Physicochem. Eng. Aspects 595 (2020) 124508, https://doi.org/10.1016/j.colsurfa.2020.124508.
[111] T.R. Shojaei, S. Soltani, M. Derakhshani, Synthesis, properties, and biomedical applications of inorganic bionanomaterials, in: B. Ahmed, J. Jaison, K.D. Michael (Eds.), Fundamentals of Bionanomaterials, Elsevier, 2022, pp. 139–174.
[112] J. Ovejero-García, Hydrogen microprint technique in the study of hydrogen in steels, J. Mater. Sci. 20 (1985) 2623–2629, https://doi.org/10.1007/BF00556094.
[113] E. Akiyama, S. Li, Electrochemical hydrogen permeation tests under galvanostatic hydrogen charging conditions conventionally used for hydrogen embrittlement study, Corros. Rev. 34 (1-2) (2016) 103–112, https://doi.org/10.1515/corrrev-2015-0049.
[114] H.Y. Ma, J.C. Wang, P. Qin, Y.J. Liu, L.Y. Chen, L.Q. Wang, L.C. Zhang, Advances in additively manufactured titanium alloys by powder bed fusion and directed energy deposition: Microstructure, defects, and mechanical behavior, J. Mater. Sci. Technol. 183 (2024) 32–62, https://doi.org/10.1016/j.jmst.2023.11.003.
[115] Y. Liu, J. Lian, X. Han, Y. Yang, H. Yuan, Hydrogen embrittlement studies of hot-stamped boron steel with different prior austenite grain sizes, J. Mater. Sci. 58 (48) (2023) 18187–18206, https://doi.org/10.1007/s10853-023-09181-0.
[116] J. Ma, Y. Zhang, J. Li, D. Cui, Z. Wang, J. Wang, Microstructure and mechanical properties of forging-additive hybrid manufactured Ti–6Al–4V alloys, Mater. Sci. Eng. A 811 (2021) 140984, https://doi.org/10.1016/j.msea.2021.140984.
[117] A. Vahedi Nemani, M. Ghaffari, A. Nasiri, Comparison of microstructural characteristics and mechanical properties of shipbuilding steel plates fabricated by conventional rolling versus wire arc additive manufacturing, Addit. Manuf. 32 (2020) 101086, https://doi.org/10.1016/j.addma.2020.101086.
[118] P. Ledwig, H. Pasiowiec, K. Cichocki, P. Lisiecka-Graca, K. Gola, R. Wróbel, B. Dubiel, Tailoring microstructure and mechanical properties of additively manufactured inconel 625 by remelting strategy in laser powder bed fusion,

MMTA 55 (7) (2024) 2485–2508, https://doi.org/10.1007/s11661-024-07412-w.
[119] Y. Liang, Q. Han, Z. Sui, Z. Zhang, H. Zhang, H. Gu, D. Wu, L. Wang, H. Liu, R. Setchi, Laser powder bed fusion of high-strength crack-free Al7075 alloy with the in-situ formation of TiB2/Al3Ti-reinforced phases and nucleation agents, Compos. B Eng. 289 (2025), https://doi.org/10.1016/j.compositesb.2024.111940.
[120] H. Zhang, Q. Han, Z. Zhang, Y. Liang, L. Wang, H. Wan, K. Lu, Z. Gao, Combined effects of carbon content and heat treatment on the high-temperature tensile performance of modified IN738 alloy processed by laser powder bed fusion, Mater. Sci. Eng., A 920 (2025) 147538, https://doi.org/10.1016/j.msea.2024.147538.
[121] A. Evangelou, R. Stylianou, A. Loizou, D. Kim, A. Liang, P. Reed, G. Constantinides, T. Kyratsi, Effects of process parameters and Scan strategy on the microstructure and density of stainless steel 316 L produced via laser powder bed fusion, J. Alloys Metall. Syst. 3 (2023) 100027, https://doi.org/10.1016/j.jalmes.2023.100027.
[122] J. Boswell, J. Jones, N. Barnard, D. Clark, M. Whittaker, R. Lancaster, The effects of energy density and heat treatment on the microstructure and mechanical properties of laser additive manufactured haynes 282, Mater. Des. 205 (2021) 109725, https://doi.org/10.1016/j.matdes.2021.109725.
[123] J. He, Y. Hu, Z. Luo, Q. Liu, S. Wang, The influence of rotation angle between layers in laser-based powder bed fusion on the hydrogen embrittlement of Ni, J. Mater. Res. Technol. 23 (2023) 3187–3195, https://doi.org/10.1016/j.jmrt.2023.01.201.
[124] M. Alnajjar, F. Christien, C. Bosch, K. Wolski, A comparative study of microstructure and hydrogen embrittlement of selective laser melted and wrought 17–4 PH stainless steel, Mater. Sci. Eng. A 785 (2020) 139363, https://doi.org/10.1016/j.msea.2020.139363.
[125] M. Neikter, M. Colliander, C. de Andrade Schwerz, T. Hansson, P. Åkerfeldt, R. Pederson, M.L. Antti, Fatigue crack growth of electron beam melted TI-6AL-4V in high-pressure hydrogen, Materials 13 (6) (2020) 1287, https://doi.org/10.3390/ma13061287.
[126] N. Zan, H. Ding, X. Guo, Z. Tang, W. Bleck, Effects of grain size on hydrogen embrittlement in a Fe-22Mn-0.6C TWIP steel, Int. J. Hydrogen Energy 40 (33) (2015) 10687–10696, https://doi.org/10.1016/j.ijhydene.2015.06.112.
[127] M. Koyama, E. Akiyama, T. Sawaguchi, D. Raabe, K. Tsuzaki, Hydrogen-induced cracking at grain and twin boundaries in an Fe-Mn-C austenitic steel, Scripta Mater. 66 (7) (2012) 459–462, https://doi.org/10.1016/j.scriptamat.2011.12.015.
[128] W. Liu, C. Liu, Y. Wang, H. Zhang, H. Ni, Effect of heat treatment on the corrosion resistance of 316L stainless steel manufactured by laser powder bed fusion, J. Mater. Res. Technol. 32 (2024) 3896–3912, https://doi.org/10.1016/j.jmrt.2024.08.194.
[129] M.C. Sow, T. De Terris, O. Castelnau, Z. Hamouche, F. Coste, R. Fabbro, P. Peyre, Influence of beam diameter on laser powder bed fusion (L-PBF) process, Addit. Manuf. 36 (2020) 101532, https://doi.org/10.1016/j.addma.2020.101532.
[130] W. Guo, R. Sun, B. Song, Y. Zhu, F. Li, Z. Che, B. Li, C. Guo, L. Liu, P. Peng, Laser shock peening of laser additive manufactured Ti6Al4V titanium alloy, Surf. Coat. Technol. 349 (2018) 503–510, https://doi.org/10.1016/j.surfcoat.2018.06.020.
[131] J. He, Q. Liu, M. He, J. Li, S. Wang, The hydrogen embrittlement of pure Ni fabricated by additive manufacturing, Int. J. Hydrogen Energy (2023), https://doi.org/10.1016/j.ijhydene.2023.01.167.
[132] Z. Fu, B. Yang, K. Gan, D. Yan, Z. Li, G. Gou, H. Chen, Z. Wang, Improving the hydrogen embrittlement resistance of a selective laser melted high-entropy alloy via modifying the cellular structures, Corros. Sci. 190 (2021) 109695, https://doi.org/10.1016/j.corsci.2021.109695.
[133] M. Alnajjar, F. Christien, V. Barnier, C. Bosch, K. Wolski, A.D. Fortes, M. Telling, Influence of microstructure and manganese sulfides on corrosion resistance of selective laser melted 17-4 PH stainless steel in acidic chloride medium, Corros. Sci. 168 (2020) 108585, https://doi.org/10.1016/j.corsci.2020.108585, 108585.
[134] J. Yoo, S. Kim, M.C. Jo, H. Park, J.E. Jung, J. Do, D.W. Yun, I.S. Kim, B.G. Choi, Investigation of hydrogen embrittlement properties of Ni-based alloy 718 fabricated via laser powder bed fusion, Int. J. Hydrogen Energy 47 (43) (2022) 18892–18910, https://doi.org/10.1016/j.ijhydene.2022.04.045.
[135] Z. Zhou, K. Zhang, Y. Hong, H. Zhu, W. Zhang, Y. He, C. Zhou, J. Zheng, L. Zhang, The dependence of hydrogen embrittlement on hydrogen transport in selective laser melted 304L stainless steel, Int. J. Hydrogen Energy 46 (29) (2021) 16153–16163, https://doi.org/10.1016/j.ijhydene.2021.02.035.
[136] D.H. Lee, B. Sun, S. Lee, D. Ponge, E.A. Jägle, D. Raabe, Comparative study of hydrogen embrittlement resistance between additively and conventionally manufactured 304L austenitic stainless steels, Mater. Sci. Eng. A 803 (2021) 140499, https://doi.org/10.1016/j.msea.2020.140499.
[137] K.M. Bertsch, A. Nagao, B. Rankouhi, B. Kuehl, D.J. Thoma, Hydrogen embrittlement of additively manufactured austenitic stainless steel 316 L, Corros. Sci. 192 (2021) 109790, https://doi.org/10.1016/j.corsci.2021.109790.
[138] J. Liu, H. Yang, L. Meng, D. Liu, T. Xu, D. Xu, X. Shao, C. Shao, S. Li, P. Zhang, Z. Zhang, Significance of melt pool structure on the hydrogen embrittlement behavior of a selective laser-melted 316L austenitic stainless steel, Materials 16 (4) (2023) 1741, https://doi.org/10.3390/ma16041741.
[139] W. Shifeng, L. Shuai, W. Qingsong, C. Yan, Z. Sheng, S. Yusheng, Effect of molten pool boundaries on the mechanical properties of selective laser melting parts, J. Mater. Process. Technol. 214 (11) (2014) 2660–2667, https://doi.org/10.1016/j.jmatprotec.2014.06.002.
[140] S. Yang, Q. Han, Y. Yin, J. Gao, Z. Zhang, Y. Gu, K.W.Q. Low, Effects of micrometer-sized TiB2 on crack mitigation, mechanical and electrochemical performance of a Ni-based alloy fabricated by selective laser melting, Opt. Laser Technol. 142 (2021) 107240, https://doi.org/10.1016/j.optlastec.2021.107240, 107240.
[141] Q. Han, Y. Gu, R. Setchi, F. Lacan, R. Johnston, S.L. Evans, S. Yang, Additive manufacturing of high-strength crack-free Ni-based hastelloy X superalloy, Addit. Manuf. 30 (2019) 100919, https://doi.org/10.1016/j.addma.2019.100919, 100919.
[142] T. Allam, X. Guo, M. Lipinska-Chwalek, A. Hamada, E. Ahmed, W. Bleck, Impact of precipitates on the hydrogen embrittlement behavior of a V-alloyed medium-manganese austenitic stainless steel, J. Mater. Res. Technol. 9 (6) (2020) 13524–13538, https://doi.org/10.1016/j.jmrt.2020.09.085.
[143] X. Shen, W. Song, S. Sevsek, Y. Ma, C. Hüter, R. Spatschek, W. Bleck, Influence of microstructural morphology on hydrogen embrittlement in a medium-Mn steel Fe-12Mn-3Al-0.05C, Metals 9 (9) (2019) 929, https://doi.org/10.3390/met9090929.
[144] J. Xu, Z. Hao, Z. Fu, X. He, H. Wang, G. Xu, Hydrogen embrittlement behavior of selective laser-melted inconel 718 alloy, J. Mater. Res. Technol. 23 (2023) 359–369, https://doi.org/10.1016/j.jmrt.2022.12.196.
[145] D. Kong, D. Zhao, G. Zhu, X. Ni, L. Zhang, W. Wu, C. Man, Y. Zhou, C. Dong, B. Sun, Heat treatment effects on the hydrogen embrittlement of Ti6Al4V fabricated by laser beam powder bed fusion, Addit. Manuf. 50 (2022) 102580, https://doi.org/10.1016/j.addma.2021.102580.
[146] C.Q. Chen, S.X. Li, H. Zheng, L.B. Wang, K. Lu, An investigation on structure, deformation and fracture of hydrides in titanium with a large range of hydrogen contents, Acta Mater. 52 (12) (2004) 3697–3706, https://doi.org/10.1016/j.actamat.2004.04.024.
[147] J. Hesketh, N. McClelland, Y. Zhang, C. Green, A. Turnbull, Influence of additive manufacturing by laser powder bed fusion on the susceptibility of alloy 718 to hydrogen embrittlement, Corros. Eng. Sci. Technol. 56 (6) (2021) 565–574, https://doi.org/10.1080/1478422X.2021.1921336.
[148] H. Cheng, H. Luo, Z. Pan, X. Wang, Q. Zhao, Y. Fu, X. Li, Effects of laser powder bed fusion process parameters on microstructure and hydrogen embrittlement of high-entropy alloy, J. Mater. Sci. Technol. 155 (2023) 211–226, https://doi.org/10.1016/j.jmst.2022.12.074.
[149] Z. Zhang, G. Obasis, R. Morana, M. Preuss, Hydrogen assisted crack initiation and propagation in a nickel-based superalloy, Acta Mater. 113 (2016) 272–283, https://doi.org/10.1016/j.actamat.2016.05.003.
[150] L. Deconinck, E. Bernardo Quejido, M.T. Villa Vidaller, E.A. Jägle, K. Verbeken, T. Depover, The mechanism behind the effect of building orientation and surface roughness on hydrogen embrittlement of laser powder bed fused Ti-6Al-4V, Addit. Manuf. 72 (2023) 103613, https://doi.org/10.1016/j.addma.2023.103613.
[151] N. Sanaei, A. Fatemi, Defects in additive manufactured metals and their effect on fatigue performance: a state-of-the-art review, Prog. Mater. Sci. (2020) 100724, https://doi.org/10.1016/j.pmatsci.2020.100724, 100724.
[152] A. Yadollahi, N. Shamsaei, S.M. Thompson, A. Elwany, L. Bian, Effects of building orientation and heat treatment on fatigue behavior of selective laser melted 17-4 PH stainless steel, Int. J. Fatigue 94 (2017) 218–235, https://doi.org/10.1016/j.ijfatigue.2016.03.014.
[153] X. Lu, M. Cervera, M. Chiumenti, X. Lin, Residual stresses control in additive manufacturing, J. Manuf. Mater. Process. 5 (4) (2021) 138, https://doi.org/10.3390/jmmp5040138.
[154] F. Haftlang, H.S. Kim, A perspective on precipitation-hardening high-entropy alloys fabricated by additive manufacturing, Mater. Des. 211 (2021) 110161, https://doi.org/10.1016/j.matdes.2021.110161.
[155] S. Feng, Z. Ai, J. He, B. Yang, G. Gou, L. Han, Effect of annealing and hot isostatic pressing on the structure and hydrogen embrittlement resistance of powder-bed fusion-printed CoCrFeNiMn high-entropy alloys, Metals 13 (3) (2023) 630, https://doi.org/10.3390/met13030630.
[156] N. Kalentics, N. Sohrabi, H.G. Tabasi, S. Griffiths, J. Jhabvala, C. Leinenbach, A. Burn, R.E. Logé, Healing cracks in selective laser melting by 3D laser shock peening, Addit. Manuf. 30 (2019) 100881, https://doi.org/10.1016/j.addma.2019.100881, 100881.
[157] Q. Han, H. Gu, R. Setchi, Discrete element simulation of powder layer thickness in laser additive manufacturing, Powder Technol. 352 (2019) 91–102, https://doi.org/10.1016/j.powtec.2019.04.057.
[158] K. Hagihara, T. Nakano, Control of anisotropic crystallographic texture in powder bed fusion additive manufacturing of metals and ceramics—A review, JOM (2021), https://doi.org/10.1007/s11837-021-04966-7.
[159] S. Yang, Y. Zhang, R. Juan, Z. Li, J. Wu, S.O. Akinwamide, J. Kuva, R. V. Björkstrand, J. Lian, Effect of building orientation, thickness, and contouring on the microstructure and mechanical properties of AlSi10Mg via laser powder bed fusion, Mater. Sci. Eng., A 923 (2025) 147685, https://doi.org/10.1016/j.msea.2024.147685.
[160] W. Wu, G. He, J. Huang, A. Zhang, X. Liu, Z. Ouyang, Z. Sun, L. Guan, S. Chu, P. Li, P. Jiang, Y. Zhang, Influence of electrochemically charged hydrogen on mechanical properties of Ti–6Al–4V alloy additively manufactured by laser powder-bed fusion (L-PBF) process, Mater. Sci. Eng. A 866 (2023) 144339, https://doi.org/10.1016/j.msea.2022.144339.
[161] R. Silverstein, D. Eliezer, Hydrogen trapping in 3D-printed (additive manufactured) Ti-6Al-4V, Mater. Charact. 144 (2018) 297–304, https://doi.org/10.1016/j.matchar.2018.07.029.
[162] Q. Zhao, H. Luo, Z. Pan, H. Cheng, J. Xu, G. Duan, Y. Qin, G. Wang, Comparative study on hydrogen embrittlement resistance in additive manufactured and forged austenitic stainless steel, Addit. Manuf. 88 (2024) 104262, https://doi.org/10.1016/j.addma.2024.104262.

[163] M.Y. Panchenko, E.V. Melnikov, S.V. Astafurov, K.A. Reunova, E.A. Kolubaev, E. G. Astafurova, Hydrogen embrittlement of the low-carbon steel produced by Electron beam additive manufacturing, RuPhJ 65 (6) (2022) 966–974, https://doi.org/10.1007/s11182-022-02720-3.
[164] N.K. Mohandas, A. Giorgini, M. Vanazzi, T. Riemslag, S.P. Scott, V. Popovich, Hydrogen embrittlement of inconel 718 manufactured by laser powder bed fusion using sustainable feedstock: effect of heat treatment and microstructural anisotropy, Metals 13 (2) (2023), https://doi.org/10.3390/met13020418.
[165] J.L. Bartlett, X. Li, An overview of residual stresses in metal powder bed fusion, Addit. Manuf. 27 (2019) 131–149, https://doi.org/10.1016/j.addma.2019.02.020.
[166] H. Nishimura, T. Hojo, S. Ajito, Y. Shibayama, M. Koyama, H. Saitoh, A. Shiro, R. Yasuda, T. Shobu, E. Akiyama, Effects of residual stress on hydrogen embrittlement of a stretch-formed tempered martensitic steel sheet, ISIJ Int. 61 (4) (2021) 1170–1178, https://doi.org/10.2355/isijinternational.ISIJINT-2020-492.
[167] H.M. Alojaly, A. Hammouda, K.Y. Benyounis, Review of recent developments on metal matrix composites with particulate reinforcement, in: H. Saleem (Ed.), Reference Module in Materials Science and Materials Engineering, Elsevier, 2023.
[168] S. Shrestha, B. Wang, P. Dutta, Nanoparticle processing: understanding and controlling aggregation, Adv. Colloid Interface Sci. 279 (2020) 102162, https://doi.org/10.1016/j.cis.2020.102162.
[169] H. Sun, R. Jiao, G. An, H. Xu, D. Wang, Influence of particle size on the aggregation behavior of nanoparticles: role of structural hydration layer, J. Environ. Sci. (China) 103 (2021) 33–42, https://doi.org/10.1016/j.jes.2020.10.007.
[170] M. Zhao, S. Shen, H. Wang, L. Niu, J. Shi, Z. Chen, X. Wang, B. Lu, Effect of heat treatment on microstructure and hydrogen embrittlement of additively manufactured and cast 18Ni300 maraging steel, J. Mater. Res. Technol. 33 (2024) 9566–9579, https://doi.org/10.1016/j.jmrt.2024.12.002.
[171] P. Kürnsteiner, M.B. Wilms, A. Weisheit, B. Gault, E.A. Jägle, D. Raabe, High-strength damascus steel by additive manufacturing, Nature 582 (7813) (2020) 515–519, https://doi.org/10.1038/s41586-020-2409-3.
[172] C.J. Todaro, M.A. Easton, D. Qiu, M. Brandt, D.H. StJohn, M. Qian, Grain refinement of stainless steel in ultrasound-assisted additive manufacturing, Addit. Manuf. 37 (2021) 101632, https://doi.org/10.1016/j.addma.2020.101632, 101632.
[173] W. Gao, Y. Zhang, D. Ramanujan, K. Ramani, Y. Chen, C.B. Williams, C.C. L. Wang, Y.C. Shin, S. Zhang, P.D. Zavattieri, The status, challenges, and future of additive manufacturing in engineering, CAD 69 (2015) 65–89, https://doi.org/10.1016/j.cad.2015.04.001.
[174] A. Puzatova, P. Shakor, V. Laghi, M. Dmitrieva, Large-Scale 3D Printing for Construction Application by Means of Robotic Arm and Gantry 3D Printer: a Review, Buildings, MDPI, 2022, p. 2023, https://doi.org/10.3390/buildings12112023.
[175] Sciaky company, The EBAM® 300 series produces the largest 3D printed metal parts & prototypes in the additive manufacturing market. https://www.sciaky.com/largest-metal-3d-printer-available. (Accessed 20 October 2025).
[176] R.D. Ardika, T. Triyono, N. Muhayat, Triyono, A review porosity in aluminum welding, Procedia Struct. Integr. 33 (2021) 171–180, https://doi.org/10.1016/j.prostr.2021.10.021.
[177] J. Gu, J. Ding, S.W. Williams, H. Gu, P. Ma, Y. Zhai, The effect of inter-layer cold working and post-deposition heat treatment on porosity in additively manufactured aluminum alloys, J. Mater. Process. Technol. 230 (2016) 26–34, https://doi.org/10.1016/j.jmatprotec.2015.11.006.
[178] J.W. Elmer, G. Gibbs, The effect of atmosphere on the composition of wire arc additive manufactured metal components, Sci. Technol. Weld. Join. 24 (5) (2019) 367–374, https://doi.org/10.1080/13621718.2019.1605473.
[179] A. Horgar, H. Fostervoll, B. Nyhus, X. Ren, M. Eriksson, O.M. Akselsen, Additive manufacturing using WAAM with AA5183 wire, J. Mater. Process. Technol. 259 (2018) 68–74, https://doi.org/10.1016/j.jmatprotec.2018.04.014.
[180] T. Lehmann, D. Rose, E. Ranjbar, M. Ghasri-Khouzani, M. Tavakoli, H. Henein, T. Wolfe, A. Jawad Qureshi, Large-scale metal additive manufacturing: a holistic review of the state of the art and challenges, Int. Mater. Rev. 67 (2022) 410–459, https://doi.org/10.1080/09506608.2021.1971427.
[181] T. Hojo, E. Akiyama, H. Saitoh, A. Shiro, R. Yasuda, T. Shobu, J. Kinugasa, F. Yuse, Effects of residual stress and plastic strain on hydrogen embrittlement of a stretch-formed TRIP-aided martensitic steel sheet, Corros. Sci. 177 (2020) 108957, https://doi.org/10.1016/j.corsci.2020.108957.
[182] K.S. Derekar, A. Addison, S.S. Joshi, X. Zhang, J. Lawrence, L. Xu, G. Melton, D. Griffiths, Effect of pulsed metal inert gas (pulsed-MIG) and cold metal transfer (CMT) techniques on hydrogen dissolution in wire arc additive manufacturing (WAAM) of aluminium, Int. J. Adv. Manuf. Tech. (2020), https://doi.org/10.1007/s00170-020-04946-2/Published.
[183] K. Pourabdollah, Fouling formation and under deposit corrosion of boiler firetubes, J. Environ. Chem. Eng. 9 (1) (2021), https://doi.org/10.1016/j.jece.2020.104552.
[184] R.C. Shivamurthy, M. Kamaraj, R. Nagarajan, S.M. Shariff, G. Padmanabham, 7-Laser surface modification of steel for slurry erosion resistance in power plants, in: C.T. Kwok (Ed.), Laser Surface Modification of Alloys for Corrosion and Erosion Resistance, 2012, pp. 177–287.
[185] J. McFall, S. Simmons, R. Cox, Developing NDE Techniques for Large Cryogenic Tanks Year 2 Report, 2010.
[186] S. Kedziora, T.B. Cao, Optimum autofrettage pressure of hydrogen valve using finite element and fatigue analysis, Engineering 12 (1) (2020) 1–24, https://doi.org/10.4236/eng.2020.121001.
[187] T. Jiang, J. Zhong, X. Zhang, W. Wang, K. Guan, Hydrogen embrittlement induced fracture of 17-4 PH stainless steel valve stem, Eng. Fail. Anal. 113 (2020) 104576, https://doi.org/10.1016/j.engfailanal.2020.104576.
[188] M. König, P. Lidar, J. Engström, K. Gott, Effect of Water Chemistry on Environmentally Assisted Cracking in Alloy 600 in Simulated PWR Environments, 1999.
[189] B.O. Omiyale, P. Kayode Farayibi, Additive manufacturing in the oil and gas industries, Anal. Tech. Szeged. 14 (1) (2020) 9–18, https://doi.org/10.14232/analecta.2020.1.9-18.
[190] S. Claire, How is 3D printing used in the nuclear power sector?. https://www.3dnatives.com/en/3d-printing-nuclear-power-sector-020320235/, 2023. (Accessed 20 October 2025).
[191] Z. Free, M. Hernandez, M. Mashal, K. Mondal, A review on advanced manufacturing for hydrogen storage applications, Energies 14 (24) (2021) 8513, https://doi.org/10.3390/en14248513.
[192] R.K. Ahluwalia, J.K. Peng, T.Q. Hua, Cryo-compressed hydrogen storage, in: A.B. Ram B. Gupta, T. Nejat Veziroğlu (Ed.), Compendium of Hydrogen Energy, Woodhead Publishing, pp. 119–145.
[193] A. Züttel, Materials for hydrogen storage, Mater. Today 6 (9) (2003) 24–33, https://doi.org/10.1016/S1369-7021(03)00922-2.
[194] E. Zhang, W. Zhang, T. Lv, J. Li, J. Dai, F. Zhang, Y. Zhao, J. Yang, W. Li, H. Zhang, Insulating and robust ceramic nanorod aerogels with high-temperature resistance over 1400 °C, ACS Appl. Mater. Interfaces 13 (17) (2021) 20548–20558, https://doi.org/10.1021/acsami.1c02501.
[195] B. Saleh, J. Jiang, R. Fathi, T. Al-hababi, Q. Xu, L. Wang, D. Song, A. Ma, 30 years of functionally graded materials: an overview of manufacturing methods, applications and future challenges, Compos. B Eng. 201 (2020) 108376, https://doi.org/10.1016/j.compositesb.2020.108376, 108376.
[196] A. Verma, A. Kapil, D. Klobčar, A. Sharma, A Review on Multiplicity in Multi-Material Additive Manufacturing: Process, Capability, Scale, and Structure, Materials (2023) 5246, https://doi.org/10.3390/ma16155246.
[197] X. Zhang, Y.h. Chueh, C. Wei, Z. Sun, J. Yan, L. Li, Additive manufacturing of three-dimensional metal-glass functionally gradient material components by laser powder bed fusion with in situ powder mixing, Addit. Manuf. 33 (2020) 101113, https://doi.org/10.1016/j.addma.2020.101113, 101113.
[198] D. Han, C. Yang, N.X. Fang, H. Lee, Rapid multi-material 3D printing with projection micro-stereolithography using dynamic fluidic control, Addit. Manuf. 27 (2019) 606–615, https://doi.org/10.1016/j.addma.2019.03.031.
[199] K.C. Kim, A.D. Kulkarni, J.K. Johnson, D.S. Sholl, Large-scale screening of metal hydrides for hydrogen storage from first-principles calculations based on equilibrium reaction thermodynamics, Phys. Chem. Chem. Phys. 13 (15) (2011) 7218–7229, https://doi.org/10.1039/c0cp02950e.
[200] S.M. Jo, Electrospun nanofibrous materials and their hydrogen storage, in: J. Liu (Ed.), Hydrogen Storage, IntechOpen, 2012, p. 181, 181.
[201] B.R. Betzler, B.J. Ade, A.J. Wysocki, M.S. Greenwood, J.J.W. Heineman, P. C. Chesser, P.K. Jain, F. Heidet, A. Bergeron, Advanced manufacturing for nuclear core design. International Conference on Physics of Reactors: Transition to a Scalable Nuclear Future, PHYSOR 2020, EDP Sciences - Web of Conferences, 2020, pp. 97–104, https://doi.org/10.1051/epjconf/202124701011.
[202] A.R. Oliveira, A.L. Jardini, E.G.D. Conte, Effects of cutting parameters on roughness and residual stress of maraging steel specimens produced by additive manufacturing, https://doi.org/10.1007/s00170-020-06309-3/Published.
[203] E. Maleki, S. Bagherifard, M. Bandini, M. Guagliano, Surface post-treatments for metal additive manufacturing: progress, challenges, and opportunities, Addit. Manuf. 37 (2021) 101619, https://doi.org/10.1016/j.addma.2020.101619.
[204] G. Strano, L. Hao, R.M. Everson, K.E. Evans, Surface roughness analysis, modelling and prediction in selective laser melting, J. Mater. Process. Technol. 213 (4) (2013) 589–597, https://doi.org/10.1016/j.jmatprotec.2012.11.011.
[205] C. Wang, K. Han, X. Liu, Y. Zhu, S. Liang, L. Zhao, M. Huang, Z. Li, First-principles study of hydrogen-vacancy interactions in CoCrFeMnNi high-entropy alloy, J. Alloys Compd. 922 (2022) 166259, https://doi.org/10.1016/j.jallcom.2022.166259.
[206] S.-H. Li, D.-H. Lee, Y. Zhao, U. Ramamurty, Hydrogen-induced softening and embrittlement in 316L stainless steel fabricated using laser-powder bed fusion, Acta Mater. 274 (2024), https://doi.org/10.1016/j.actamat.2024.119959.
[207] M. Soleymani, V. Mostafavi, M. Hebert, S. Kelouwani, L. Boulon, Hydrogen propulsion systems for aircraft, a review on recent advances and ongoing challenges, Int. J. Hydrogen Energy 91 (2024) 137–171, https://doi.org/10.1016/j.ijhydene.2024.10.131.
[208] M.M. Peksen, D. Wen, Dynamic behaviour of cryogenic liquid hydrogen storage tanks, Int. J. Hydrogen Energy 149 (2025), https://doi.org/10.1016/j.ijhydene.2025.150028.
[209] P. Shantharaj, A.S. Prashanth, M. Nagaral, V. Bharath, V. Auradi, K. Dharshan, Microstructure, tensile and compression behaviour of B4C particles reinforced Al7075 matrix composites, Mater. Today proc. 52 (2022) 1135–1139, https://doi.org/10.1016/j.matpr.2021.11.008.
[210] F.H. Brahim Necib, Stress analysis of an aircraft fuselage with and without portholes using CAD/CAE process, J. Aeronaut. Aerospace. Eng. 4 (1) (2015), https://doi.org/10.4172/2168-9792.1000138.
[211] G. Chai, T. Antonsson, S. Wessman, L. Ryde, Microstructures and hydrogen embrittlement fracture mechanisms in 17-4PH martensitic stainless steel, Procedia Struct. Integr. 42 (2022) 155–162, https://doi.org/10.1016/j.prostr.2022.12.019.
[212] C. Testa, L. Greco, J. Bosschers, Marine propeller shaft loading analysis in moderate oblique-flow conditions, Ocean Eng 262 (2022), https://doi.org/10.1016/j.oceaneng.2022.112199.

[213] M.B. Djukic, V.S. Zeravcic, G. Bakic, A. Sedmak, B. Rajicic, Hydrogen embrittlement of low carbon structural steel, Procedia Mater. Sci. 3 (2014) 1167–1172, https://doi.org/10.1016/j.mspro.2014.06.190.
[214] X.H. Shi, A.P. Teixeira, J. Zhang, C. Guedes Soares, Reliability analysis of a ship hull structure under combined loads including slamming loading, Ships Offshore Struct. 11 (3) (2014) 300–315, https://doi.org/10.1080/17445302.2014.987438.
[215] S.E. Hirdaris, W. Bai, D. Dessi, A. Ergin, X. Gu, O.A. Hermundstad, R. Huijsmans, K. Iijima, U.D. Nielsen, J. Parunov, N. Fonseca, A. Papanikolaou, K. Argyriadis, A. Incecik, Loads for use in the design of ships and offshore structures, Ocean Eng. 78 (2014) 131–174, https://doi.org/10.1016/j.oceaneng.2013.09.012.
[216] S.K. Sharma, R.C. Sharma, J. Lee, In situ and experimental analysis of longitudinal load on carbody fatigue life using nonlinear damage accumulation, Int. J. Damage Mech. 31 (4) (2021) 605–622, https://doi.org/10.1177/10567895211046043.
[217] Y. Guo, Y. Wei, Z. Yang, C. Huang, X. Wu, Q. Yin, Nonlinearity of interfaces and force transmission of bolted flange joints under impact loading, Int. J. Impact Eng. 109 (2017) 214–223, https://doi.org/10.1016/j.ijimpeng.2017.06.012.
[218] Y. Chen, S. Zhao, H. Ma, H. Wang, L. Hua, S. Fu, Analysis of hydrogen embrittlement on aluminum alloys for vehicle-mounted hydrogen storage tanks: a review, Metals 11 (2021) 1303, https://doi.org/10.3390/met11081303.
[219] J.A. Gómez, D.M.F. Santos, The status of On-Board hydrogen storage in fuel cell electric vehicles, Designs 7 (4) (2023), https://doi.org/10.3390/designs7040097.